STATISTICAL ANOMALY DETECTION AND DIAGNOSTICS WITH APPLICATIONS IN POWER SYSTEMS

by

YANG XIAOZHOU

(B.Eng., National University of Singapore)

A THESIS SUBMITTED FOR THE DEGREE OF

DOCTOR OF PHILOSOPHY

in the

DEPARTMENT OF INDUSTRIAL SYSTEMS ENGINEERING AND MANAGEMENT

NATIONAL UNIVERSITY OF SINGAPORE

2021

Supervisor:
Associate Professor Chen Nan

To my delicious friends

Acknowledgments

Some acknowledgments.

Contents

Abstract

Statistical Anomaly Detection and Diagnostics with Applications in Power Systems

by

Yang Xiaozhou

Doctor of Philosophy in Industrial Engineering

National University of Singapore

There is increased volatility in the power system with the addition of unconventional generation sources and loads. Power system condition monitoring is one of the critical tasks for reliable delivery of high-quality electricity. In particular, online transmission line outage detection and localization over the entire network enable timely corrective action to be taken and prevent a local event from cascading into a large scale blackout. Line outage detection aims to detect a transmission line outage as soon as possible after it happened while the localization is focused on accurately identifying the disconnected line or lines. The penetration of Phasor Measurement Unit (PMU) technology allows the collection of high-resolution time-synchronized real-time data on the network. Using voltage phase angle data collected from the PMUs, we propose a dynamic online transmission line outage detection and localization scheme developed from the full AC power flow model and statistical change detection theory. Traditional outage detection methods rely heavily on the simplified DC power flow model which largely ignores system dynamics over time. The method proposed can capture system dynamics since the time-variant and nonlinear nature of the power system are retained. The method is online friendly and scales to large networks because of the algorithm's low computational cost. Through extensive simulation study on both the detection delay and localization accuracy, the scheme is proven to be more effective than existing methods. The standard IEEE 9-bus and 39-bus test power systems are used in the

simulation study. The method proposed could be incorporated into the current wide-area monitoring system and help to improve system operators' situational awareness in real time, thus improving the resilience of the power system. As an extension from this work, we would further investigate the problem by considering an economic constraint on the number of PMUs that can be installed on the power network as well as the optimal placement of available PMUs.

List of Figures

List of Tables

Chapter 1

Introduction

Critical infrastructures (CIs) are essential to lives, livelihoods, and the proper functioning of societies. CIs are networks of inter- or independent man-made systems and processes that produce and distribution a continuous flow of essential goods and services [1]. Five main types of CIs are electrical power systems, gas networks, water networks, transportation networks, and telecommunication systems. They have many common characteristics. For example, they are networks with large number of nodes and links, span extensively in geographical scale, and have developed capabilities for near real-time monitoring [2].

The central theme of this thesis revolves around electrical power systems, in particular, novel methods for the protection of them. Electricity is needed in almost every aspect of the modern society. It is especially important as other CIs are increasingly reliant on it as an input. Traditional power systems consist of three functional parts: generation, transmission, and distribution. Generation systems generate electrical power to meet the overall demand; power is then delivered through loss-minimizing transmission lines to downstream areas; finally, end consumers such as residential and office buildings receive usable power supply via distribution systems.

To ensure a continuous supply of high-quality electricity, power system operators work around the clock to keep the system running smoothly. However, this is not an easy feat. Power systems are extremely complex because of the extensive geographical scale, fast dynamics, and high operational standards in place. A real power system typically spans across multiple states in the United States or cities and countries in Europe's case. Within such a system, a plethora of dynamics is always in play. Thousands of power generators, transformers, electric lines and etc. could be interacting with each other at any moment. Three major power grids of the United States consist of 275,000 kilometers of high-voltage transmission lines and over nine million kilometers of low-voltage distribution lines; in Europe, four major grids are comprises of four million transformers and 10 million kilometers of distribution lines. At the same time, the integration of distributed energy resources, smaller power sources such as batteries and renewable energy sources, introduces increasing volatility to modern power systems [3].

1.1 Motivation

Ensuring a reliable electricity supply is a challenging task. To achieve it, fast and accurate abnormal event detection and identification (D&I) is necessary to contain system failures in time and minimize the impact of such events. Abnormal events in power systems create disturbances which are different from a normal operating condition. Depending on the cause and duration, such disturbances may or may not lead to acute or cascading failures. Given the complexity of the system, there are many types of disturbances that could happen [4]. Among them, power transmission line outage receives a significant amount of attention from both the research community and the industry. Power line outages can happen frequently due to reasons like adverse weather conditions, component wear and tear, or vandalism. The increased research activities in power line outage D&I can be attributed to two reasons. One is the urgent need to improve system operators' real-time situational awareness. On the other hand, the emergence of phasor measurement unit (PMU) technology makes numerous real-time monitoring and control applications possible.

1.1.1 Real-time Situational Awareness

Real-time situational awareness about the system, e.g., changes in operating conditions and external system contingencies, enables system operators to promptly identify and respond to abnormal events [5]. From a contingency point of view, delayed information regarding system faults might allow localized faults cascade into large-scale blackouts [6]. For example, one of the common contributing factors of the 2003 Northeast and 2011 Southwest blackout was that the operators were not alerted in time about external outage contingencies, e.g., tripping of a critical transmission line [7]. One of the challenges about real-time monitoring is that line outage dynamics can manifest in a time scale of milliseconds [8]. Traditional supervisory control and data acquisition (SCADA) system is not able to capture these dynamics since it reports at a rate of one measurement every several seconds [9].

1.1.2 Emergence of Phasor Technology

Synchrophasors are time-synchronized numbers that represent both the magnitude and phase angle of the sine waves found in electricity, e.g., voltage phasor or current phasor. PMUs are devices capable of recording such synchrophasor samples when installed across the power grid with high precision, high fidelity and GPS time stamps [6]. An industry-grade PMU can measure voltage phasors on the bus with a total vector error of less than 1%, and with a reporting rate of 30 to 60 samples per second. The rising prevalence of PMUs makes many real-time monitoring, protection, and control applications possible since they can measure system states at a much higher frequency than traditional SCADA system. As a result, many consider PMU technology as the key to grid modernization. PMU technologies are actively studied for tasks such as power oscillation monitoring [10], abnormal event detection [11, 12], and dynamic state and parameter estimation [13, 14]. For a comprehensive review of PMU applications in the power system, readers can refer to [6].

1.2 Challenges

However, there are also challenges that need to be addressed before realizing the full potential of PMU technology for line outage D&I. One is the real-time computational challenge. As mentioned, outage D&I is most wanted for enhancing operators' real-time awareness. Consequently, a common goal for any D&I scheme is to keep computational cost low enough for real-time processing and extracted information rich enough for useful analytics. In particular, PMU's high sampling rate means that data processing has to be fast. Furthermore, a realistic power system usually contains hundreds of lines and substations. Therefore, the proposed D&I scheme has to be efficient to handle real-time processing of fast streaming data and scalable to large dimensions. A specific challenge for outage line identification is the inherent combinatorial nature of potential outage locations. An outage can happen at one or multiple transmission lines; the total number is in general not known a priori. For example, for a system with L transmission lines, the solution space for identification consists of 2^L location combinations. An exhaustive search is only possible for small systems. The proposed scheme has to overcome this challenge for any realistic power system implementation.

Another challenge for line outage D&I is that sensor deployment is limited in number. PMU is the foundation for many D&I schemes. However, PMUs are only progressively adopted by energy companies. Installing PMUs also means the whole data communication, processing, and storage infrastructure behind the technology, which is expensive. Separately, there have been many research works suggesting a full PMU deployment is not needed for many applications [15]. Therefore, one must consider a limited PMU deployment in the system, i.e., some parts are not observable, when designing a D&I scheme. As a consequence, a limited PMU deployment, in terms of the number and location, impacts outage detection scheme's effectiveness. In particular, line outages which happen far away from buses with PMUs would register mild signals in the data, leading to a longer detection delay or missed detection [16]. It remains a challenge to design a detection scheme robust to the location of the PMUs and outages. A limited coverage also leads to increased identification difficulty. Pre- and post-outage states at different parts of the system need to be used to discriminate outage of one location from another. Having some unobservable buses means that signatures of certain outages might not be captured. This lost of information might lead to some outages of different locations being indistinguishable from one another [17–19]. Hence, an effective outage identification scheme has to overcome the ambiguity issue caused by a limited PMU deployment.

1.3 State of the Art

We review the state-of-the-art research works in power system real-time line outage detection and identification using PMU data.

1.3.1 Outage Detection

Research that deals with the problem of detecting a line outage as fast as possible after it happened can be summarized from two aspects: the approach and the type of system dynamics considered. Outage detection research by their approaches are first reviewed. Then, from a perspective of system dynamics, current work is reviewed to find further important research gap. Finally, research work that focus on outage line identification is reviewed.

1.3.1.1 By Approach

Most works of line outage detection using PMU data can be classified by the two approaches taken. One is a data-driven approach where no or very little physical knowledge about the system is required [20–22]. On the other hand, many take a hybrid approach where first-principle models are incorporated with data-driven methods [23–31].

Data-driven Approach Using principal component analysis (PCA), Xie *et al.* builds a lower-dimensional representation of observable bus states from available PMU data under an outage-free condition [20]. Once online data is obtained, the reconstruction error of PMU data by the representation is used as the basis to flag abnormal events such as an outage. Similarly, using a moving-window PCA on normal condition system-wide frequency data, Rafferty *et al.* design a Hotelling's T^2 control chart to detect and classify multiple types of abnormal frequency events [21]. Hosur and Duan proposed to construct an observation matrix based on frequency difference between buses under a normal condition by modeling the network as a linear time-invariant (LTI) system [22]. An alarm is raised whenever the underlying null space of the observation matrix changes due to different types of events, such as topology change or forced oscillation. The method is not limited to line outage, but requires a window of samples to reflect a null space change. Without a model for the power system based on physical laws, these data-driven schemes are flexible enough to detect both outages and other abnormal events. However, they often face difficulties when the events have a low signal-to-noise ratio, e.g., outages with mild phase angle disturbances. The hybrid approach, on the other hand, augments PMU data with physical system information to improve the detection performance under such conditions.

Hybrid Approach Based on Ohm's law, Jamei *et al.* show that the correlation matrix between voltage and current measurements of a pair of buses has rank one under normal condition [24]. An alarm is raised once this the error of the approximation based on rank-1 assumption significantly deviates from zero. The authors devised both a local and central rule for abnormal event detection. The formulation also considers the unique condition of unbalanced phases in a distribution grid. However, currents and voltages at both ends of the line are assumed to be known. Also, the focus of the detection scheme is on deriving the signal without a systematic approach to designing a monitoring scheme that balances detection speed and false alarm rate. Also based on Ohm's law, Ardakanian *et al.* monitor the discrepancy between measured and computed quasi-steady state current phasors using recovered admittance matrix [26]. A separate line of work makes use of the direct current (DC) power flow model. Using pre- and post-outage steady-state bus voltage phase angle difference, outage detection is formulated as a quickest change detection problem solved by sequential likelihood ratio testing [30, 32]. This line of work does not require all buses to be monitored by a PMU. However, the steady-state approximation would not be sufficient at describing the actual system behavior following an outage.

There is minimal work on detection schemes that allow unobservable buses and consider system transient response to an outage.

1.3.1.2 By System Dynamics

In addition to the usage of physical system models, most state-of-the-art works on outage detection can also be categorized by the type of power system transient dynamics, the evolution of system states following a disturbance, considered in their problem formulation. A review from this perspective allows new research direction to be discovered.

Steady State The first group models power systems based on the quasi-steady state assumption where no transient dynamics are considered [25–28, 30, 33]. Their detection methods assume that the system is in a quasi-steady state both before and after the outage. Under this assumption, the DC power flow model, which simplifies many details of the system, is usually used as the starting point for detection scheme design. However, transient dynamics can often last up to several seconds and are non-negligible in real-time operations [34]. Therefore, this approach may not be adequate at describing the actual system behavior.

Approximate Dynamics The second group relaxes the quasi-steady state assumption and attempts to account for the post-outage transient dynamics. That means, the voltage and current profiles of buses and transmission lines are assumed to be time-variant rather than static, especially after an outage. Building on the sequential testing approach in [30], Rovatsos *et al.* modeled the dynamic evolution of post-outage voltage phase angles using a series of participation factor matrices. The matrices quantify the impact of an outage on phase angles based on system topology and current states [31]. Similarly, using voltage angles, a generalized likelihood ratio-based detection scheme is developed using the AC power flow model in Chapter 3 of this thesis. Separately, monitoring is also done on low-dimensional subspaces derived from PMU measurements that capture post-outage transient dynamics. Methods such as principal component analysis (PCA) [20], moving-window PCA [21], and hidden Markov model (HMM) [35] are used. Jamei *et al.* proposed to monitor the correlation matrix obtained from adjacent bus voltage and current phasors [24]; Hosur and Duan proposed to monitor that of the observation matrix obtained during outage-free operation [22]. These methods can capture post-outage dynamics in a more realistic way than those assuming steady-state operations. However, all of them rely on system algebraic variables, e.g., bus voltage and current. Power generator state variables can better characterize the system's transient response to the power imbalance created by the outage.

Generator Dynamics The third group models the power system as a dynamical system, utilizing both the measurable algebraic variables and hidden generator state variables. Using the swing equation, a second-order differential equation describing the dynamics of generators, Pan *et al.* formulated outage diagnosis as a sparse recovery problem solved by an optimization algorithm [36]. Similarly, using the swing equation, a visual observer network is constructed to monitor line admittance changes by a parameter identification method [37]. Both works focus on the outage diagnosis problem, i.e., localization and parameter estimation. However, a systematic detection scheme is the prerequisite for such tasks and needs to be developed.

There is limited work on line outage detection considering generator dynamics in a partially observed network. No work brings together generator state and power flow algebraic variable information for systematic outage detection.

1.3.2 Outage Identification

An early detection of line outage may not lead to better system protection if the location of the outage line(s) are not known. Research on outage lines identification has also thrived in the past twenty years, mainly taking three directions. Research work that focus on identifying outage lines by estimating post-outage line parameters is reviewed first. Then, those with a machine learning approach and expected phase angle change approach are reviewed.

Parameter Recovery Approach Power system line outage identification in general can be formulated as a line parameter change identification problem. An outage of line ℓ corresponds to the change when the line admittance of ℓ drops to zero. When post-outage system parameters could be estimated, a comparison with pre-outage baseline information could reveal outage locations. Some attempted to solve this problem by recovering changed line parameter. Yu *et al.* uses the power flow equations to formulate line parameters as unknown regression coefficients and recover them via total least squares method in [38] and by considering changing baseline conditions in [39]. Another approach focuses on the system admittance matrix, which depends on line-bus connection information, and recover the elements of the matrix via matrix decomposition and adaptive lasso [26, 32]. These methods can both locate multiple line outages and recover post-outage system parameters. However, they either require a full PMU deployment or smart meter measurements, e.g., power injection and voltage measurements for the power flow approach, current and voltage measurements for the admittance matrix approach at all buses.

Machine Learning Approach It is however more realistic to assume only part of the system is observable by PMUs or smart meters as stated in challenges previously. Operating under this assumption, researchers mainly seek to solve line outage identification problem, i.e., locate outage lines. They generally takes two directions. The first one is reviewed here. Machine learning-based approach has been gaining traction in recent years. This line of work leverages easily accessible simulated power system outage data, extract useful information from them, and trains an outage classifier in a supervised learning setting. The classifier then identifies most likely outage locations when given a new set of system data. Classifical supervised learning techniques such as multinomial logistic regression classifiers are used [12, 40]. Recently, Li *et al.* and Zhao *et al.* propose to use convolutional and variational inference-augmented neural network, a versatile machine learning technique, to identify tripped lines [41, 42]. This approach exploits the ability of these algorithms to learn an excellent representation of line outages. They are powerful at locating multiple line outages with limited PMUs. However, their performance depend on generalizable and usually massive training data.

Expected Angle Change Approach The second approach that does not demand a full PMU deployment on power system is the expected bus voltage phase angle change formulation. Different from the machine learning approach, this line of work does not depend on training data neither. Instead, well-known physical laws governing power systems are utilized to construct a “dictionary” of how voltage phase angles might change following any outage. That knowledge is then used to decide where outage might have happened after post-outage system data have been collected. This dictionary of patterns of angle change is usually based on either the DC power flow model [17, 27, 28, 43–45] or the AC model [18]. Outage line identification is then formulated into an unknown sparse vector recovery problem or a pattern-matching problem. For example, the outage status of all lines are formulated as an unknown vector recovered by optimization methods such as orthogonal matching pursuit, mixed-integer programming, cross-entropy optimization, and matrix decomposition [17, 43–45]. Also, Tate and Overbye and Enriquez *et al.* use correlation between measurement data and expected phase angle data to identify the most likely outage locations [18, 27]. However, the usage of the DC power flow model potentially creates system representations with fidelity inadequate for accurate single- and multiple-line outage identification. All but Enriquez *et al.* consider the AC power flow model. However, their approach requires both voltage and current information. Overall, despite demonstrated effectiveness by the above works, the identification performance degrades significantly when a limited number of PMUs are available or when multiple-line outages are considered.

Therefore, given an outage detection timestamp, multiple-line outage identification problem still remains difficult when (1) massive generalizable training data is not available or feasible, (2) only a portion of the system buses are equipped with PMUs, (3) only bus voltage phasor information is used.

1.4 Thesis Organization

This thesis is devoted to the development of novel power system line outage detection and identification methods by addressing the challenges and research gaps mentioned in previous sections. In particular, the rest of this thesis is organized as follows.

Chapter 2 gives background information on how power systems as complex networks could be modeled and simulated. These information will be repeated referenced in the rest of this thesis. Specifically, AC power flow model that describes system algebraic states, i.e. bus voltage, are introduced along with relevant power system physical quantities. Then, dynamic simulation procedure of power systems and the open-source software package used to do it are introduced. These describe how line outage data are simulated and obtained using standard IEEE test power systems.

Chapter 3 describes a novel hybrid approach to outage detection where a power system model is the basis for the statistical detection method. A time-variant small-signal relationship between net active power and nodal voltage phase angles is derived from the AC power flow model. Outage detection is then formulated as a statistical distribution change detection problem. A generalized likelihood ratio detection scheme is implemented to detect the outage at a pre-specified false alarm rate.

In Chapter 4, a unified detection framework that monitors both generator dynamics and load bus power changes using a limited number of PMUs is developed. System transient dynamics are tracked through nonlinear state estimation via a particle filter (PFs). A statistical change detection scheme is constructed by monitoring the PF-predicted system output's compatibility with the expected normal-condition measurement. When an outage happens, a significant reduction in the compatibility triggers an alarm, detecting the outage in the quickest time possible.

Chapter 5 describes a new framework of multiple-line outage identification based on power system sensitivity analysis and sparse regression methods considering line diagnosabilities. Using readily available system topology and parameter information, a signature map of line outages based on AC power flow sensitivity analysis is build in advance. Outage identification problem is then formulated into an underdetermined sparse regression problem that accommodates any a priori unknown number of simultaneous line outages. Crucially, clusters of lines whose outages are indistinguishable under the given PMU placement are identified and augmented with the initial result to improve identification accuracy.

Chapter 6 concludes this thesis and discusses future research directions.

Chapter 2

Power System Background

This Chapter provides brief background information on power system modeling and simulation. In particular, relevant physical quantities and physical laws governing power systems are introduced in Section 2.1. Power system simulation and PMU data collection are introduced in Section 2.2.

2.1 Power System Model

Sinusoidal physical quantities in power systems at constant frequency are phasors characterized their maximum value and phase angle. For example, voltage phasor can be represented by

$$v(t) = \mathrm{V}_{\mathrm{max}} e^{j\theta}\,, \tag{2.1}$$

where $\mathrm{V}_{\mathrm{max}}$ is the maximum value and θ is voltage phase angle. The effective value, V, is

$$\mathrm{V} = \frac{\mathrm{V}_{\mathrm{max}}}{\sqrt{2}}\,, \tag{2.2}$$

and voltage phasor can also be written as

$$V = \mathrm{V}e^{j\theta} = \mathrm{V}\angle\theta = \mathrm{V}\cos\theta + j\mathrm{V}\sin\theta\,, \tag{2.3}$$

in the so-called exponential, polar, and rectangular form. The same can be written for current phasor I. The complex power in power systems can be obtained by the multiplying voltage and current phasor:

$$S = VI^* \tag{2.4}$$

$$= \mathrm{P} + j\mathrm{Q}\,, \tag{2.5}$$

where I^* is the complex conjugate of I. P is real or active power and Q is reactive power.

A power system can be modeled as a network with N buses of $\mathcal{N} = \{1, \ldots, N\}$ connected by L transmission lines of $\mathcal{L} = \{1, \ldots, L\}$. The flow of real and reactive power in the network can be characterized by a set of non-linear algebraic equations called the AC power flow model. This set of equations describes the relationship between net active power injection (P), net reactive power injection (Q), voltage magnitude (V), and voltage phase angle (θ) governed by Kirchhoff's circuit laws. They can be written as:

$$\mathrm{P}_m = \mathrm{V}_m \sum_{n=1}^{N} \mathrm{V}_n \mathrm{Y}_{mn} \cos(\theta_m - \theta_n - \alpha_{mn}) \,, \tag{2.6a}$$

$$\mathrm{Q}_m = \mathrm{V}_m \sum_{n=1}^{N} \mathrm{V}_n \mathrm{Y}_{mn} \sin(\theta_m - \theta_n - \alpha_{mn}) \,, \tag{2.6b}$$

for bus $m = 1, 2, \ldots, N$ [34]. Y_{mn} is the magnitude of the $(m, n)_{th}$ element of the bus admittance matrix $\boldsymbol{Y}$ when the complex admittance is written in the exponential form, i.e.

$$\mathrm{Y}_{mn} e^{j\alpha_{mn}} = G_{mn} + jB_{mn} \,, \tag{2.7}$$

where G_{mn} and B_{mn} are the conductance and susceptance of line ℓ connecting bus m and n. Elements of the bus admittance matrix corresponding to a baseline condition are usually known and this condition is also assumed for the rest of this thesis. For a large system, $\boldsymbol{Y}$ is usually a sparse matrix since any single bus only has a few incident buses, i.e., $\mathrm{Y}_{mn} = 0$ if bus m and bus n are not connected. The system topology is embedded in the admittance matrix $\boldsymbol{Y}$. In particular, the admittance matrix is constructed by

$$\boldsymbol{Y} = \mathbf{A}[\mathbf{y}]\mathbf{A}^T \tag{2.8}$$

where $\mathbf{A}$ is the bus to branch incidence matrix with columns representing lines and rows as buses. $\mathbf{A}^T$ is the transpose of $\mathbf{A}$. For the l_{th} line transmitting power from bus m to bus n, the l_{th} column of the matrix $\mathbf{A}$ has 1 and -1 on the m_{th} and n_{th} position and 0 everywhere else. $[\mathbf{y}]$ is the diagonal matrix with individual line admittances on the diagonal.

2.2 Power System Simulation

For a bus equipped with PMU, V and θ are measured and available.

Chapter 3

Outage Detection Using Approximate Dynamics

3.1 Introduction

The main contributions of this work can be summarized in two aspects. Firstly, the power system model retains the non-linear and time-varying characteristics of system transient response that follows after the outage. The system is not assumed a quasi-steady state immediately after the disruption. In fact, from the dynamic outage simulation, it is observed that the transient response could last over 10 seconds. Secondly, the proposed GLR detection scheme can deal with the trade-off between system-wide false alarm rate and detection delay. The ability to decide among different detection thresholds gives operators the flexibility to cater to their system needs. The detection scheme is also computationally efficient, therefore friendly for online implementation in a large network.

The remainder of this paper is organized as follows. Section 4.1 describes the power system model and the statistical model used to characterize system behaviors before and after the outage. Then, dynamic detection and identification scheme is developed in Section 4.1.2. Effectiveness of the proposed scheme on simulation data of two test power systems are reported and discussed in Section 4.3. In Section 5.5 we conclude the paper with two future research directions.

3.2 Problem Formulation

3.2.1 Power System Model

Without the loss of generality, we assume bus 1 is the reference bus. This bus serves as the angular reference to all other buses, and its phase angle is set to 0°. The voltage magnitude at the reference bus is also set to 1.0 per unit (p.u.). Let $\mathbf{P}$, $\mathbf{Q}$, $\boldsymbol{\theta}$, and $\mathbf{V}$ represent the $(N-1)$-dimensional column vectors of net active power, net reactive power, voltage angles and magnitudes respectively at all buses except the reference bus. Taking a derivative with respect to time t on both sides of (5.1), we obtain

$$\begin{bmatrix} \frac{\partial \mathbf{P}}{\partial t} \\ \frac{\partial \mathbf{Q}}{\partial t} \end{bmatrix} = \left[\begin{array}{c|c} \mathbf{J}_1 & \mathbf{J}_2 \\ \hline \mathbf{J}_3 & \mathbf{J}_4 \end{array}\right] \cdot \begin{bmatrix} \frac{\partial \boldsymbol{\theta}}{\partial t} \\ \frac{\partial \mathbf{V}}{\partial t} \end{bmatrix}, \tag{3.1}$$

where $\mathbf{J}_i, i = 1, \ldots, 4$ are the four submatrices of the AC power flow Jacobian with

$$\mathbf{J}_1 = \frac{\partial \mathbf{P}}{\partial \boldsymbol{\theta}}, \mathbf{J}_2 = \frac{\partial \mathbf{P}}{\partial \mathbf{V}}, \mathbf{J}_3 = \frac{\partial \mathbf{Q}}{\partial \boldsymbol{\theta}}, \mathbf{J}_4 = \frac{\partial \mathbf{Q}}{\partial \mathbf{V}}. \tag{3.2}$$

In the usual operating range of relatively small angles, real power systems exhibit much stronger interdependences between $\mathbf{P}$ and $\boldsymbol{\theta}$ and between $\mathbf{Q}$ and $\mathbf{V}$ than those between $\mathbf{P}$ and $\mathbf{V}$ and between $\mathbf{Q}$ and $\boldsymbol{\theta}$ [46]. By neglecting $\mathbf{J}_2$ and $\mathbf{J}_3$, (5.3) reduces to the decoupled AC power flow equations where the changes in voltage angles and magnitudes are not coupled, i.e. $\mathbf{J}_2 = \mathbf{J}_3 = \mathbf{0}$. Therefore, we obtain a small-signal time-variant model describing the relationship between active power mismatches and the changes in voltage angles:

$$\frac{\partial \mathbf{P}}{\partial t} \approx \mathbf{J}_1(\boldsymbol{\theta}) \frac{\partial \boldsymbol{\theta}}{\partial t}. \tag{3.3}$$

From here onwards, we drop the subscript 1 from $\mathbf{J}_1$. The off-diagonal and diagonal elements of the $\mathbf{J}$ matrix can be derived from Eqn (5.1a) respectively:

$$\frac{\partial \mathrm{P}_m}{\partial \theta_n} = \mathrm{V}_m \mathrm{V}_n \mathrm{Y}_{mn} \sin\left(\theta_m - \theta_n - \alpha_{mn}\right)\,, m \neq n\,, \tag{3.4a}$$

$$\frac{\partial \mathrm{P}_m}{\partial \theta_m} = -\sum_{\substack{n=1 \\ n \neq m}}^{N} \mathrm{V}_m \mathrm{V}_n \mathrm{Y}_{mn} \sin\left(\theta_m - \theta_n - \alpha_{mn}\right)\,. \tag{3.4b}$$

Note that $t \in [0, \infty)$ is implicit in the continuous-time quantities $\mathbf{P}, \mathbf{V}$ and $\boldsymbol{\theta}$. Accordingly, we define their discrete counterparts as $\mathbf{P}_k, \mathbf{V}_k$ and $\boldsymbol{\theta}_k$ at time t_k for $k = 1, 2, \ldots$. For PMU devices with a sampling frequency of 30 Hz, $\Delta t = t_k - t_{k-1} = 1/30$ s. A first-order difference discretization by Euler's formula can approximate (5.2) by:

$$\Delta \mathbf{P}_k = \mathbf{J}(\boldsymbol{\theta}_{k-1}) \Delta \boldsymbol{\theta}_k\,, \tag{3.5}$$

where $\Delta \mathbf{P}_k = \mathbf{P}_k - \mathbf{P}_{k-1}$ and $\Delta \boldsymbol{\theta}_k = \boldsymbol{\theta}_k - \boldsymbol{\theta}_{k-1}$, i.e. the active power mismatch and difference between two consecutive angle measurements. We have derived a time-variant relationship between variations in phasor angles and net active power on buses. The key feature of our model lies in the $\mathbf{J}$ matrix in (3.5). The matrix changes with $\boldsymbol{\theta}$, which in turn changes with time. Therefore, it retains the non-linear and dynamic nature of the AC power system.

Methods relying on a static relationship between $\Delta \mathbf{P}$ and $\Delta \boldsymbol{\theta}$ make three further assumptions about the system [27, 30]: 1) flat voltage profile, i.e. $\mathrm{V}_m \approx \mathrm{V}_n \approx 1.0$ p.u.; 2) approximately homogeneous bus angles across the network, i.e. $\cos(\theta_m - \theta_n) \approx 1, \sin(\theta_m - \theta_n) \approx 0$; 3) reactive property of a line is much more significant than its resistive property, i.e. $B_{mn} \gg G_{mn}$. Under these assumptions, (5.2) reduces to

$$\frac{\partial \mathbf{P}}{\partial t} \approx -\mathbf{B} \frac{\partial \boldsymbol{\theta}}{\partial t}\,, \tag{3.6}$$

where $\mathbf{B}$ is the imaginary component of $\boldsymbol{Y}$. While line resistances in transmission systems are generally one order of magnitude smaller than reactances, this is not usually the case for distribution systems [47]. Also, a static model may not be accurate enough to reflect the transient behavior

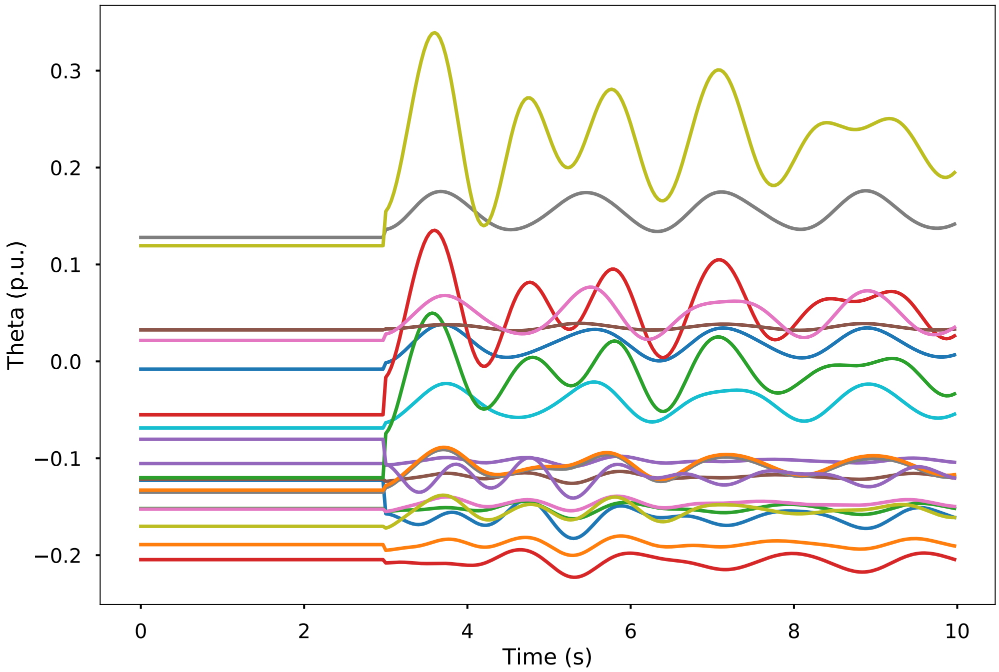

Figure 3.1: *The progression of bus voltage phase angles after an outage at $t = 3$ s, where each line corresponds to one bus. The steady-state bus angle balance is severely distorted during the transient response phase.*

after an outage since the homogeneous angles assumption might be violated [48]. We routinely encounter this phenomenon in our dynamic simulation. For example, in Fig. 3.1, the balance between voltage angles is severely distorted following an outage, e.g., at around $t = 3.75$ s. Furthermore, the duration of transient dynamics is non-negligible for real-time detection purposes. Therefore, to reflect the dynamic behavior in a timely and accurate manner, $\mathbf{J}$ matrix in (3.5) is updated by real-time streaming PMU data.

3.2.2 Statistical Model

For a balanced steady-state power system with no active power mismatch, we have $\mathbf{P}_0 = 0$. Within a short period of time, net active power fluctuates around zero as the generators respond to random changes in electricity demand. Therefore, we can model the trajectory of $\mathbf{P}$ as a Brownian motion with drift $\mathbf{0}$ and variance $\sigma^2 t\mathbf{I}$ which is a continuous-time stochastic process: $\{\mathbf{P}_t : t \in [0, \infty)\}$. σ^2 is pre-determined and $\mathbf{I}$ is an identity matrix of appropriate dimension. One of the implications of a Brownian motion is that their independent increment, i.e. $\Delta\mathbf{P}_k = \mathbf{P}_{t_k} - \mathbf{P}_{t_{k-s}}$, follows a multivariate Gaussian distribution with mean $\mathbf{0}$ and variance $\sigma^2(t_k - t_{k-s})\mathbf{I}$ [49]. In particular, taking $s = 1$, we have $t_k - t_{k-s} = \Delta t$ and

$$\Delta\mathbf{P}_k \sim \mathcal{N}(\mathbf{0}, \sigma^2 \Delta t \mathbf{I})\,. \tag{3.7}$$

Since σ^2 is pre-determined, we can replace $\sigma^2\Delta t$ by σ^2 for notational simplicity. Rearranging the variables in (3.5), we have

$$\Delta\boldsymbol{\theta}_k = \mathbf{J}(\boldsymbol{\theta}_{k-1})^{-1}\Delta\mathbf{P}_k\,. \tag{3.8}$$

Therefore, we can characterize bus angle variations by

$$\Delta\boldsymbol{\theta}_k \sim \mathcal{N}(\mathbf{0}, \sigma^2(\mathbf{J}(\boldsymbol{\theta}_{k-1})^T\mathbf{J}(\boldsymbol{\theta}_{k-1}))^{-1})\,. \tag{3.9}$$

From (3.9), we see that the angle variations at time k are characterized by the structure of $\mathbf{J}$ and the angle values at $t = k - 1$. Let $\mathcal{L}$ represent the set of all possible combinations of outages, e.g., single-line outage, double-line outage. When an outage $\ell \in \mathcal{L}$ happens, the grid topology and the bus admittance matrix changes. The new bus admittance matrix $\boldsymbol{Y}_\ell$ induces a new $\mathbf{J}_\ell$, and therefore, a new distribution of $\Delta\boldsymbol{\theta}_k$. There is a one-to-one correspondence between an outage scenario and a distribution of $\Delta\boldsymbol{\theta}_k$. Furthermore, we assume that the outage is persistent, i.e., tripped lines are not restored in the time under consideration. We also assume that the outage would not result in any islanding in the network, i.e., no part of the system is isolated from the main grid.

In light of the above characterization, we adopt a hypothesis testing framework to detect the distribution change in $\Delta\boldsymbol{\theta}_k$:

$$H_0 : \Delta\boldsymbol{\theta}[k] \sim \mathcal{N}(\mathbf{0}, \sigma^2(\mathbf{J}_0^T\mathbf{J}_0)^{-1})\,, \tag{3.10a}$$

$$H_1 : \Delta\boldsymbol{\theta}[k] \sim \mathcal{N}(\mathbf{0}, \sigma^2(\mathbf{J}_\ell^T\mathbf{J}_\ell)^{-1})\,, \ell \in \mathcal{L}\,, \tag{3.10b}$$

for $k = 1, 2, \ldots$. The null hypothesis is that there is no outage, and the corresponding Jacobian is $\mathbf{J}_0$. The alternative hypothesis is that there is an outage scenario ℓ, where the corresponding Jacobian is $\mathbf{J}_\ell$. If we reject the null hypothesis at time τ, then the distribution of $\Delta\boldsymbol{\theta}[k]$ has changed, and the outage is detected. The detailed procedure of real-time detection under this framework is described in Section 4.1.2.

A common challenge for PMU applications is that not all buses are equipped with a PMU. Here we adapt the previous formulations to a limited PMU deployment. Suppose K PMUs are installed where $K < N$. Given a selection matrix $\mathbf{S} \in \{0, 1\}^{(K \times N)}$ that selects K observable buses from the complete set of N buses, observable bus angle data is

$$\boldsymbol{\theta}_k^o = \mathbf{S}\boldsymbol{\theta}_k \,, \tag{3.11}$$

where $\mathbf{S}$ is a diagonal matrix of size $(K \times N)$ and entries equal to 0 or 1. The corresponding angle variations and Jacobian matrix are

$$\begin{aligned} \Delta\boldsymbol{\theta}_k^o &= \mathbf{S}\Delta\boldsymbol{\theta}_k \,, &(3.12)\\ \mathbf{J}^o(\boldsymbol{\theta}_{k-1}^o) &= \mathbf{S}\mathbf{J}(\boldsymbol{\theta}_{k-1}^o)\mathbf{S}^T \,. &(3.13) \end{aligned}$$

Therefore, $\Delta\boldsymbol{\theta}_k^o$ is a K-dimensional vector and $\mathbf{J}^o(\boldsymbol{\theta}_{k-1}^o)$ is a $(K \times K)$-dimensional matrix. To obtain the hypothesis testing framework in (3.10), we replace $\Delta\boldsymbol{\theta}_k, \mathbf{J}_0,$ and $\mathbf{J}_\ell$ by $\Delta\boldsymbol{\theta}_k^o, \mathbf{J}_0^o,$ and $\mathbf{J}_\ell^o$ respectively.

3.2.3 Outage Detection Scheme

We have formulated the outage detection as a problem of distribution change detection under a hypothesis testing framework in Section 3.2.2. In general, under normal conditions, system outputs follow a common distribution with a probability density function f_0. At some unknown time τ, the system condition changes, and the density function changes to f_1. We wish to design a scheme where an alarm is raised once a monitoring statistic $W(\cdot)$ crosses a pre-defined threshold of c. The two key design aspects are: 1) how to compute the monitoring statistic, $W(\cdot)$; 2) how to determine the detection threshold, c. The monitoring statistic will be close to zero under a normal condition and increase unboundedly if a change happens. The detection threshold needs to be specified to meet a particular false alarm rate constraint.

We adopt a GLR approach originally proposed by [50] to design the detection scheme. The scheme repeatedly evaluates the likelihood of a normal condition against the likelihood of an abnormal condition. In our problem, bus angle variations are not independent samples since the distribution at time k is influenced by bus angles at time $k-1$ as shown in (3.9). However, $\Delta\boldsymbol{\theta}_k$ can be regarded as a conditionally independent random variable with density function $f_0(\cdot|\boldsymbol{\theta}_{k-1})$ under H_0 in (3.10a) and, after an outage, with density function $f_\ell(\cdot|\boldsymbol{\theta}_{k-1})$ under H_1 in (3.10b). For every new data $\Delta\boldsymbol{\theta}_k$, we test H_0 against H_1 for some outage scenario $\ell \in \mathcal{L}$ using a log-likelihood ratio test statistic. In particular, let

$$Z_k(\ell) = \ln \frac{f_\ell(\Delta\boldsymbol{\theta}_k|\boldsymbol{\theta}_{k-1})}{f_0(\Delta\boldsymbol{\theta}_k|\boldsymbol{\theta}_{k-1})} \tag{3.14}$$

be the log-likelihood ratio of an outage scenario ℓ at time k. $Z_k(\ell)$ is positive if the likelihood of a change is larger than that of a normal condition. Then the test statistic is:

$$G_k = \max\left\{0,\ \max_{1\le i\le k}\ \max_{\ell\in\mathcal{L}} \sum_{j=i}^{k} Z_j(\ell)\right\}. \tag{3.15}$$

and the GLR detection scheme will raise an alarm at the time:

$$D = \inf\left\{k \ge 1 : G_k \ge c\right\}. \tag{3.16}$$

Since the time and location of the outage are not known a priori, they are replaced by their maximum likelihood estimates. Schemes of the form involving searching through the maximum over time ($1 \le i \le k$) and over likelihood ($\sum_{j=i}^{k} Z_j(\ell)$) are referred to as the GLR schemes. Such schemes have optimal properties in terms of their detection performance. Let $E_{H_0}(D)$ be the expectation of time of alarm when there is no outage, i.e., mean time to a false alarm. Suppose c is chosen such that the scheme satisfies a certain false alarm rate, $E_{H_0}(D) \geq \gamma\{1+o(1)\}$. For conditionally independent data, Lai has proved that the detection rule (3.16) is asymptotically optimal in the sense that among all rules T with $E_{H_0}(T) \geq \gamma\{1+o(1)\}$, it minimizes the worst-case detection delay as defined by

$$\overline{E}_{H_1}(T) = \sup_{\tau\geq 1} \operatorname{ess\,sup} E^{(\tau)} \left[(T-\tau+1)^+ | \boldsymbol{\theta}_1, \cdots, \boldsymbol{\theta}_{\tau-1}\right] , \tag{3.17}$$

as the outage time $\tau \to \infty$ [51].

For the actual online implementation, we use a recursive formulation of the GLR scheme. Note that G_k in (3.15) can be rewritten as

$$\begin{aligned} G_k &= \max\left\{0, \max_{\ell\in\mathcal{L}} \max_{1\leq i\leq k} \sum_{j=i}^{k} Z_j(\ell)\right\} , \\ &= \max_{\ell\in\mathcal{L}} \max\left\{0, \max_{1\leq i\leq k} \sum_{j=i}^{k} Z_j(\ell)\right\} , \\ &= \max_{\ell\in\mathcal{L}} W_{\ell,k} . \end{aligned} \tag{3.18}$$

where in the first step we have switched the position of the two inner max operators since the overall maximum is not affected [52]. Also, in the last step,

$$W_{\ell,k} = \max\left\{0, W_{\ell,k-1} + Z_k(\ell)\right\} , \tag{3.19}$$

an equivalent recursive form of the term $\max\limits_{1\leq i\leq k} \sum_{j=i}^{k} Z_j(\ell)$ in G_k. Therefore, for every scenario ℓ, we just need to keep track of the monitoring statistic W_{k-1} at the previous time step and obtain the log-likelihood ratio Z_k at the current time step. $Z_k(\ell)$ can be found analytically by

$$Z_k(\ell) = \ln|\mathbf{J}_\ell| - \ln|\mathbf{J}_0| + \frac{1}{2\sigma^2}\Delta\boldsymbol{\theta}_k^T \left[{\mathbf{J}_0}^T\mathbf{J}_0 - {\mathbf{J}_\ell}^T\mathbf{J}_\ell\right]\Delta\boldsymbol{\theta}_k , \tag{3.20}$$

based on the multivariate Gaussian distribution likelihood function. Using the recursive formulation, the stopping time is

$$D = \inf\left\{k \geq 1 : \max_{\ell\in\mathcal{L}} W_{\ell,k} \geq c\right\} . \tag{3.21}$$

Intuitively, the threshold is crossed when the evidence against the normal condition, i.e., no outage, has accumulated to a significant level. c is a predefined threshold that controls the balance between the detection delay and the false alarm rate. A smaller c corresponds to a more sensitive scheme that may have a quicker detection but could potentially flag more normal fluctuations as outages. One advantage of using the GLR approach is that such trade-off can be systematically quantified. Following [30], given a false alarm rate constraint, c could be approximated by

$$c = \ln(ARL_0 \times p) \, , \tag{3.22}$$

where ARL_0 is the average run length to a false alarm of the scheme when no outage occurs. p is the number of PMUs installed. For example, $c = 18.43$ when $ARL_0 = 1$ day with 39 PMUs installed. With this detection delay and false alarm rate trade-off in mind, ISOs can choose a desired level of sensitivity, catering to the individual system needs, and implement it in the detection scheme through parameter c and ARL_0. A flowchart summarizing the working of the detection and identification scheme outlined in this section is shown in Fig. 3.2.

3.2.4 Additional Remarks

Setting up Outage Scenarios The one-to-one correspondence between the Jacobian and grid topology can be established by looking at how the admittance matrix is constructed in (5.7). $\boldsymbol{Y}$ is constructed from the bus incidence matrix $\mathbf{A}$ and the line admittances. For different outage scenarios, we just need to set the corresponding column of $\mathbf{A}$ to 0. For example, to set up the l_{th} line outage, we set the entries in the l_{th} column of $\mathbf{A}$ to 0 to get $\mathbf{A}_\ell$. The corresponding bus admittance matrix $\boldsymbol{Y}_\ell$ is obtained by $\boldsymbol{Y}_\ell = \mathbf{A}_\ell[\mathbf{y}]\mathbf{A}_\ell^T$. The Jacobian matrix $\mathbf{J}_\ell$ describing the post-outage system is obtained by (5.4). Therefore, no simulation or real data is needed to generate the outage scenarios to set up the monitoring scheme during offline preparation. In real applications, both the bus incidence matrix and the line admittances can be obtained based on the network topology and

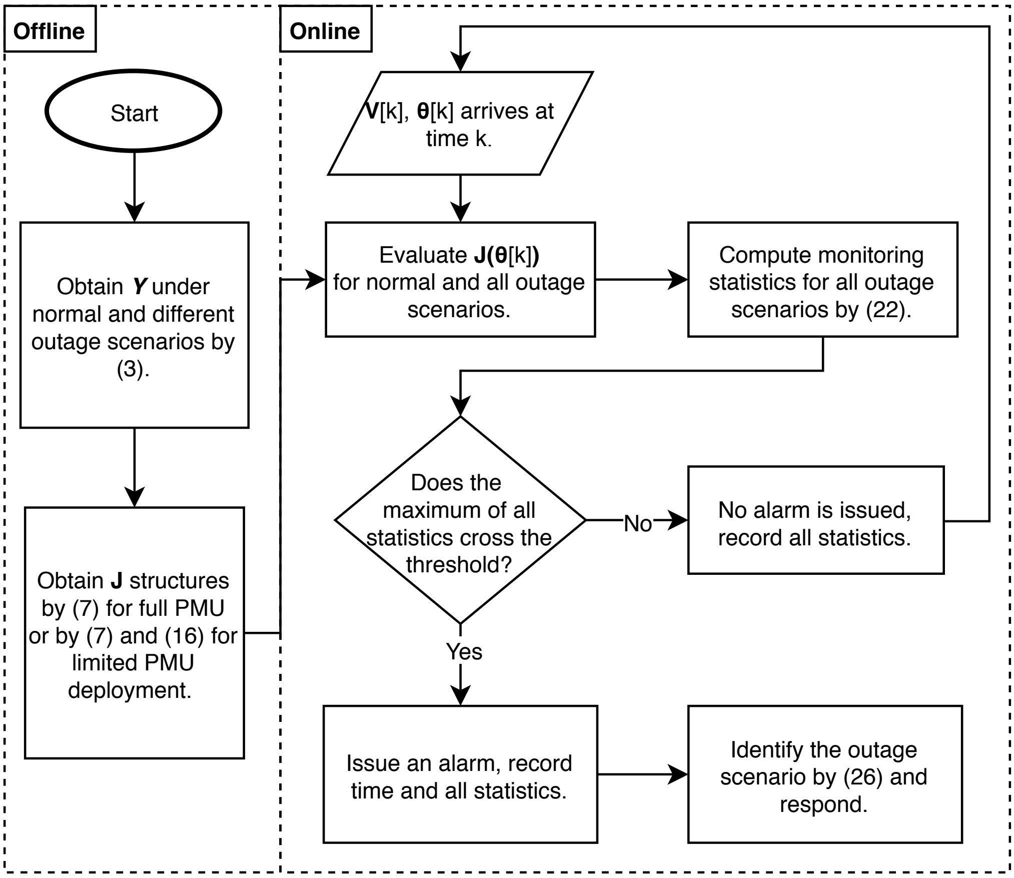

Figure 3.2: *Flowchart summarizing the proposed dynamic outage detection and identification scheme.*

data during the outage-free period. It will then be sufficient to apply the proposed method.

Inaccuracy of Jacobian Due to Unobservable Neighbor Buses For a limited PMU deployment, there may be some inaccuracies in the computed diagonal elements of $\mathbf{J}^o(\boldsymbol{\theta}^o_{k-1})$. In particular, if there is no PMU on bus n, a neighbor of bus m, measurements V_n and θ_n would not be available. Therefore, the term, $-\mathrm{V}_m\mathrm{V}_n\mathrm{Y}_{mn}\sin(\theta_m-\theta_n-\alpha_{mn})$, would not be computable and is treated as 0 for the summation in (5.4b). The issue could be alleviated by carefully designing the PMU placement (locations). One possible design rule is to make sure that each observable bus has at least one observable neighbor bus. In general, PMU locations will influence the efficiency of outage detection. It is also of interest to practitioners to find the optimal placement of PMUs so that even with limited PMUs, we can detect outages as quickly as possible. However, the placement problem is beyond the scope of this paper, and we will study this topic in our future research.

Identification of Tripped Lines Following detection, the actual lines tripped need to be identified so that follow-up, potentially automatic, actions can be taken. Since we monitor and compare the likelihood of every outage scenario online, one way to locate the tripped line(s) without any extra computation is to identify the scenarios with the top three likelihoods at the time of detection. In particular, following a detection at time D, top-three possible tripped lines can be identified as $\ell_{(1)}, \ell_{(2)}, \text{and } \ell_{(3)}$ such that:

$$W_{\ell_{(1)},D} \geq W_{\ell_{(2)},D} \geq W_{\ell_{(3)},D} \geq W_{\ell,D}\,, \tag{3.23}$$

for all other $\ell \in \mathcal{L}$.

3.3 Simulation Study

3.3.1 Simulation Setting

We test our detection scheme on two IEEE standard test power systems, namely 39 bus New England system [53] and 2383 bus Polish system. System transient responses following an outage are simulated using the open-source dynamic simulation platform COSMIC [54] in which a third-order machine model is used. We conduct extensive single-line outage detection and identification analysis on the 39 bus system by comparing our method to two other methods. Outages on the 2383 bus system are simulated to show that the proposed scheme can be deployed on large-scale systems as well.

We assume that the sampling frequency of PMU is 30 Hz. For every new simulation, we vary the system loads by a random percentage between

Table 3.1: Detection Thresholds Corresponding to Different Systems and False Alarm Rates

Mean Time to False Alarm (day)	Number of PMUs Installed 10	39	1000
1/24	13.89	15.25	18.50
1/4	15.68	17.05	20.29
1/2	16.38	17.74	20.98
1	17.07	18.43	21.68
2	17.76	19.12	22.37
7	19.02	20.38	23.62
30	20.47	21.83	25.08

-5% and 5% from the base-line values. Each simulation runs for 10 seconds, and the line outage takes place at the 3rd second. Active power fluctuations are assumed to be uncorrelated and have homogeneous variances where $\sigma^2 = 0.005$ in (3.10). Artificial noise is added to all sampled bus angle data, $\Delta\boldsymbol{\theta}$, to account for system and measurement noise [55]. The noises are drawn from a normal distribution with mean 0 and standard deviation equivalent to 10% of the average value of sampled $\Delta\theta$ on respective buses. Detection thresholds c in (3.21) corresponding to seven different false alarm rates are obtained by (3.22) and listed in Table 3.1.

3.3.2 Simulation Results

3.3.2.1 39 Bus New England System

The 39 bus system has 39 buses, 10 generators, and 46 transmission lines. We conduct extensive simulation studies for the full PMU deployment and limited PMU deployment scenario. For the latter case, we assume that PMUs are installed on bus 2, 3, 7, 9, 11, 13, 16, 17, 19, and 21. In total, 3000 random simulations of outages at line 1 to 36 are studied, except for line 22 as its outage leads to two separate networks and line 37 to line 46 since they are the only line connecting the generator bus to the system. The proposed method can detect outages instantaneously in most cases with a full PMU deployment. Due to the page constraint, we only present the

Table 3.2: Time-step breakdown of the detection scheme for processing each new measurement

Step	Action	Time Required
0	Receive new sample	0
1	Evaluate $\mathbf{J}_0$ and $\mathbf{J}_\ell$ for $\ell \in \mathcal{L}$	1 ms
2	Compute outage statistics $\mathbf{W}_\ell$ for $\ell \in \mathcal{L}$	0.227 ms
3	Check if max $\mathbf{W}_\ell$ for $\ell \in \mathcal{L}$ exceed c	0

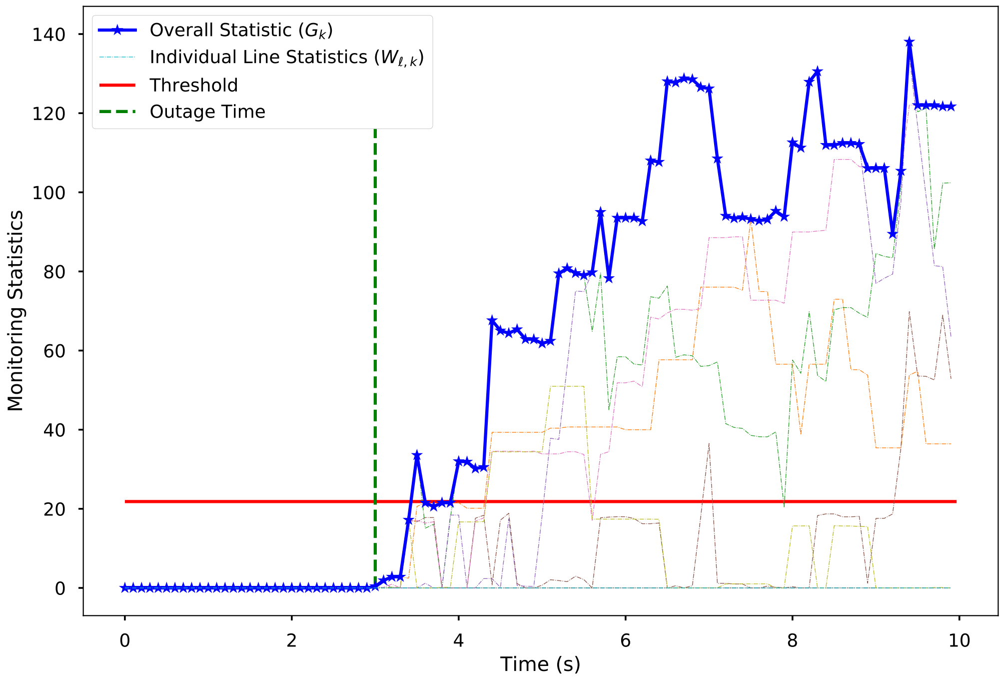

Figure 3.3: *Progression of monitoring statistics for line 10 outage. Individual line statistics are represented by faded dash lines of various colors. The blue solid line is the overall statistic.*

detection results of a limited PMU deployment here.

We use an outage at line 10 to demonstrate the typical working of the detection scheme. Table 3.2 shows a time-step breakdown for the scheme when processing each new measurement. The execution time is obtained by running the algorithm on a personal laptop with a 2.9 GHz Intel Core i5 processor. Note that a new measurement is collected every 33 ms. Fig.

3.3 shows the progression of the individual scenario statistics as well as the overall statistic. After the outage (3rd second), individual statistics start to deviate from zero. The overall monitoring statistic rises quickly, too, since it is the maximum of all individual statistics. The scheme issues an alarm when the overall statistic crosses the threshold at time 3.5 seconds. In this case, the scheme records a detection delay of 0.5 seconds. Among all 35 individual statistics representing different outage scenarios, only some have values significantly larger than 0, while most of them stay close to 0 as they are deemed as unlikely scenarios by the detection scheme.

Also, as we do not have restrictions on the transient stability of the post-outage system, our algorithm does not require bounded signals for outage detection, and it works equally well in stable and unstable scenarios. In fact, an outage that creates an unstable system is easier to detect since it produces stronger signals than those that do not. This is illustrated by a separate simulation example included in the Appendix.

Detection Performance Fig. 3.4 shows the empirical distribution of detection delays under seven false alarm rates. A more stringent false alarm rate corresponds to a detection scheme with longer delays on average. For example, the scheme with an $ARL_0 = 1/24$ day detects much more outages within 0.25 seconds than the one with $ARL_0 = 30$ days. These differences are not significant. Hence, the proposed scheme's performance based on detection delay is not overly sensitive to different false alarm rates.

We have also studied the detection performance across different line outages. There are clear variations in terms of detection delay among those detected outages. These variations can be largely attributed to the PMU placement and the grid topology.

For outages with almost zero detection delay, they are lines where either PMUs are installed on both ends of the line, e.g., line 3, 21, and 23, or one PMU is connected to the line, e.g., line 20, 25, and 27. Signals can be readily picked up by nearby PMUs. On the other hand, the absence of PMU nearby may have contributed to the longer detection delays. In

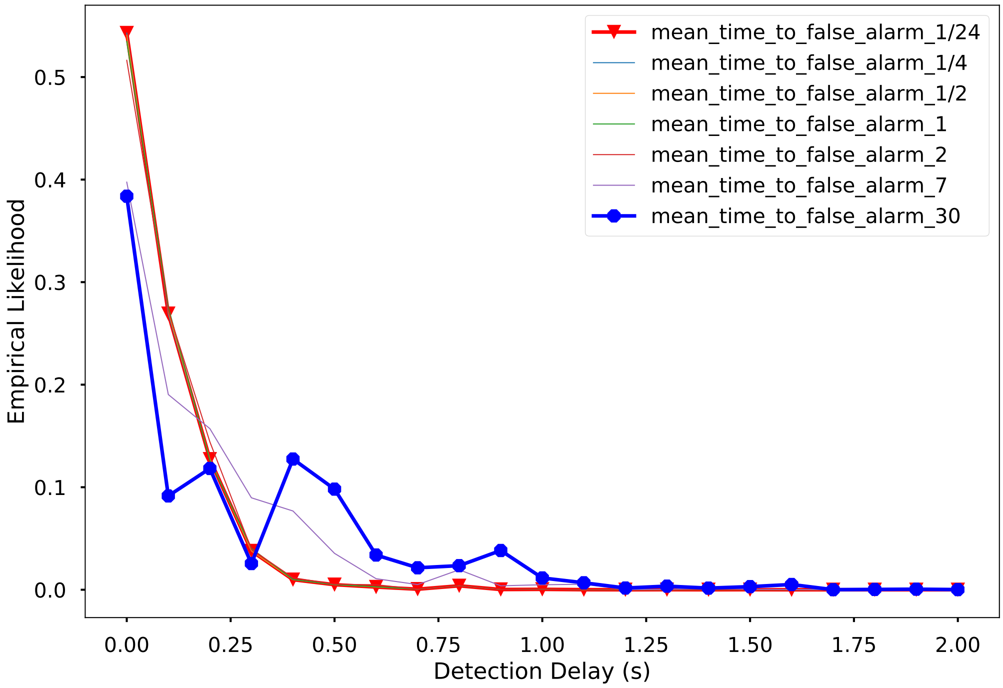

Figure 3.4: *Comparison of the empirical distribution of detection delays in seconds under different false alarm rates. The number in the label is the number of days until a false alarm.*

particular, there are no PMUs available on either end of line 9, 10, 28, 32, 33, and 34. These outage signals have to be detected by sensors far away from the location. Fig. 3.3.2.1 summarizes the comparison.

Another factor is the power grid topology. The scheme recorded shorter delays for line 2, 14, 15, and 30. It is observed that these outages produced severe disturbances. Line 2, 14, and 15 connect to a generator bus, and line 30 connects a subnetwork to the main network. On the other hand, outages at line 5, 11, 13, and 26 produced weaker and shorter disturbances, which are more difficult to detect. Consequently, they recorded longer detection delays. See Fig. 3.3.2.1 for the comparison.

Comparison with Other Methods We compared the proposed method's outage detection performance with two other methods. The line outages considered here are line 26, 27, and 34. Other methods considered here

Table 3.3: Comparison of Detection Delay (s) of Three Different Line Outages Under Different Detection Schemes

		Mean Time to False Alarm (day)			
Line	Scheme	1/24	2	7	30
26	DC - full	9.9908	9.9908	9.9908	9.9908
	DC - limited	–	–	–	–
	Ohm's Law - limited	2.8150	3.0963	3.1406	3.9333
	AC - limited	0.1001	0.1005	0.3300	0.3489
27	DC - full	4.5398	4.5398	4.5398	4.5398
	DC - limited	–	–	–	–
	Ohm's Law - limited	3.3044	3.5000	3.6900	3.8630
	AC - limited	0.0012	0.0012	0.0026	0.0039
34	DC - full	0.1801	0.1801	0.1801	0.1801
	DC - limited	–	–	–	–
	Ohm's Law - limited	1.5811	2.9250	3.2014	3.6788
	AC - limited	0.0879	0.0879	0.1558	0.4994

are the static detection method based on the DC power flow model in [30], under a full and limited PMU deployment, and the CUSUM-type central rule based on Ohm's law in [24], with a limited PMU deployment. The placement of 10 PMUs is the same for all methods. For the CUSUM scheme in [24], parameters are chosen to satisfy the same false alarm rates in Table 3.1 based on formula in [56]. The respective detection delays are summarized in Table 4.1. A dash means a missed detection. It can be seen that our proposed method, "AC - limited", is consistently faster at detecting outages than the other methods.

Identification Performance We analyzed the identification performance by comparing the true outage line with the identified line. The results are shown in Fig. 3.6. True outage lines are listed on the vertical axis, and the lines identified are on the horizontal axis. Cell color represents the empirical likelihood of identification of different lines. Therefore, a perfect identification scheme would have all diagonal cells equal to 1 and 0 everywhere else. As seen from the figure, most lines can be accurately identified under a full PMU deployment. As for the 10-PMU case, around half of the outages can

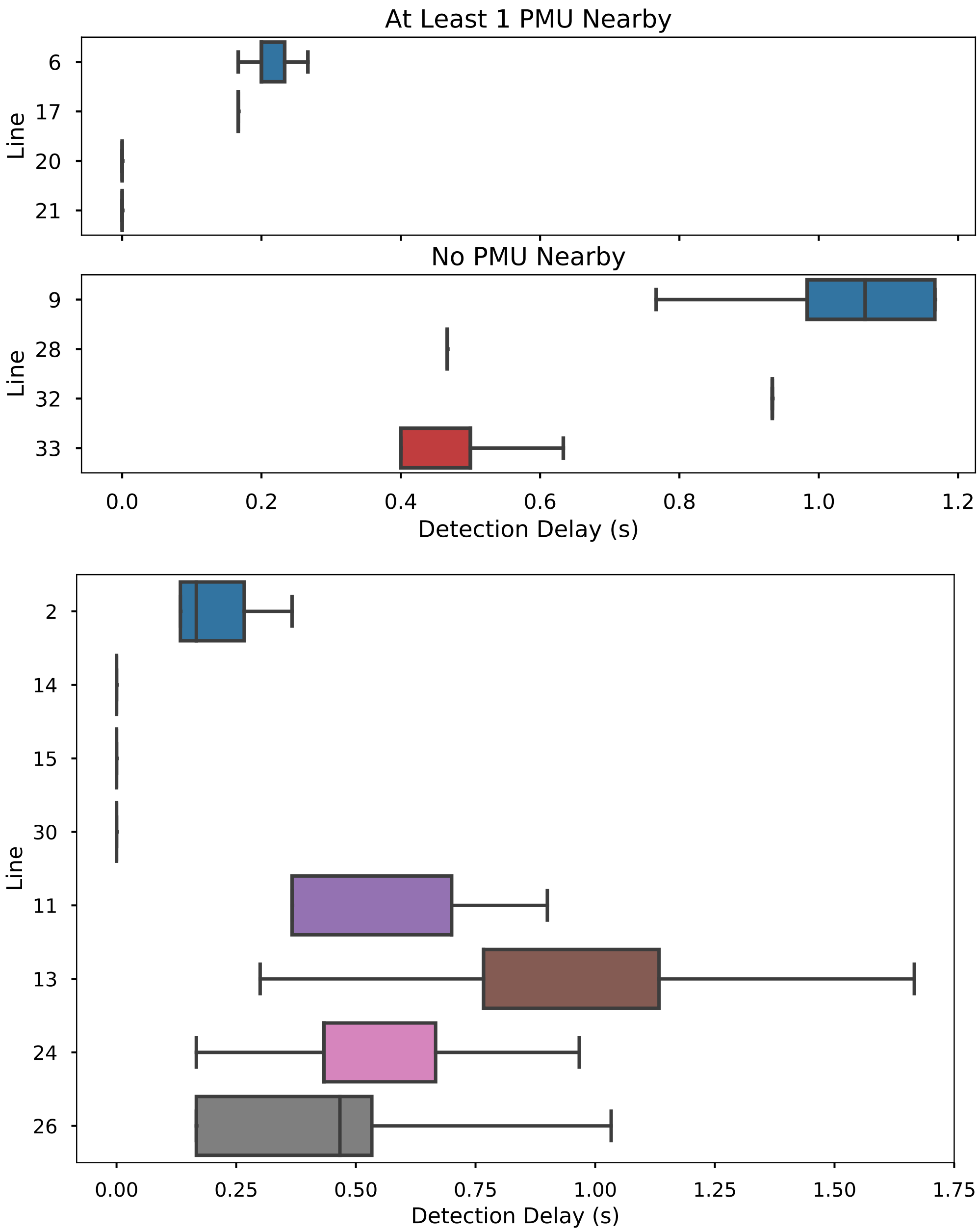

[]

[]

Figure 3.5: *Boxplot of the empirical distributions of detection delay in seconds for (a) lines with at least 1 PMU nearby and those without, (b) lines at different topological locations.*

be identified with a high probability. When the scheme misses the true outage line, it often misidentifies the adjacent line as tripped. Systematic biases created by the unavailability of PMUs on certain buses may have

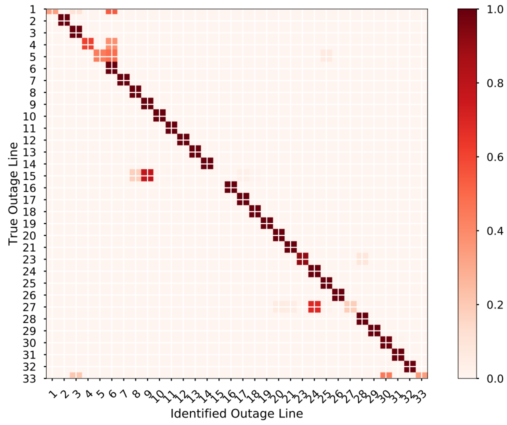

[39 PMUs] [10

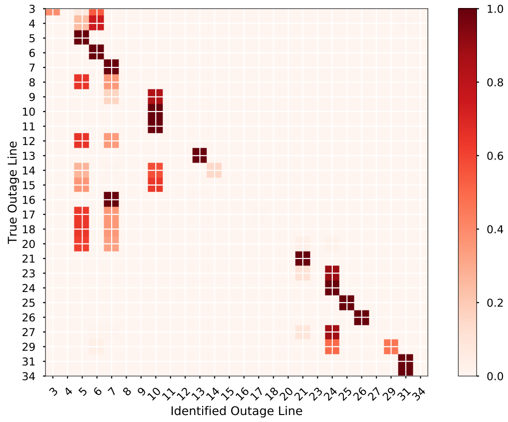

PMUs]

Figure 3.6: *Heat map showing the identification accuracy of the proposed method in the 39 bus system with (a) a full PMU deployment and (b) 10 PMUs deployed.*

contributed to the inaccuracies. This suggests installing more PMUs or inspecting the identified line and all its neighboring lines could improve the localization accuracy.

3.3.3 2383 Bus Polish System

To show that the proposed dynamic detection scheme can be deployed in a system with realistic network size, outages in the 2383 bus system are studied. This test system has 2383 buses and 2896 transmission lines. 1000 PMUs are assumed to be placed at randomly selected locations in the system. Eight different line outages are simulated to test the proposed detection scheme. Detection delay results corresponding to four different

Table 3.4: Detection Delay (s) of Eight Different Line Outages in 2383 Bus System with 1000 PMUs Deployed

	Mean Time to False Alarm (day)			
Line	1/24	2	7	30
600	4.6667	4.6667	4.6667	4.6667
700	1.3667	1.3667	1.3667	1.3667
750	4.9000	4.9000	4.9000	4.9000
800	1.3667	1.3667	6.7667	6.7667
900	–	–	–	–
1000	–	–	–	–
1050	1.3667	1.3667	1.3667	1.3667
1650	–	–	–	–

false alarm rates are reported in Table 3.4. Considering the size of the system, detecting a single-line outage is much more difficult. Therefore, delays experienced are considerably longer than those in the 39 bus system. There are also several undetected outages.

3.4 Conclusion

In this work, we developed a real-time dynamic line outage detection and identification scheme based on the AC power flow model and GLR scheme. We derived a time-variant small-angle relationship between bus voltage angles and active power injections. We obtained the pre- and post-outage statistical models of the angle variations. The proposed scheme is effective in both detection and identification. It is also scalable, as seen from the results in the 2383 bus system.

For further research, we would investigate the optimal number and placement of a limited number of PMUs. As seen from Section 4.3, there is a varying level of detection delays due to PMU placement. The number of PMUs needed to achieve a certain level of identification accuracy is also worth investigating. We would also consider incorporating generator dynamics into our system model, where we hope the detailed physical model could provide an even better direction for outage detection and identification.

3.5 Appendix

3.5.1 Unstable Post-Outage System

We show a simulation example to illustrate the working of the detection scheme when the outage creates an unstable and transient system. In the 39-bus system, line 37 outage creates large disturbances throughout the system, as shown in Figure 3.7. From the onset of the outage to the end of the simulation, voltage phase angles at most buses show no significant sign of stabilization. The detection scheme is able to detect the outage immediately, as shown in Figure 3.8. In this case, the monitoring statistic records a significantly large value, indicating that the strength of the signals is strong.

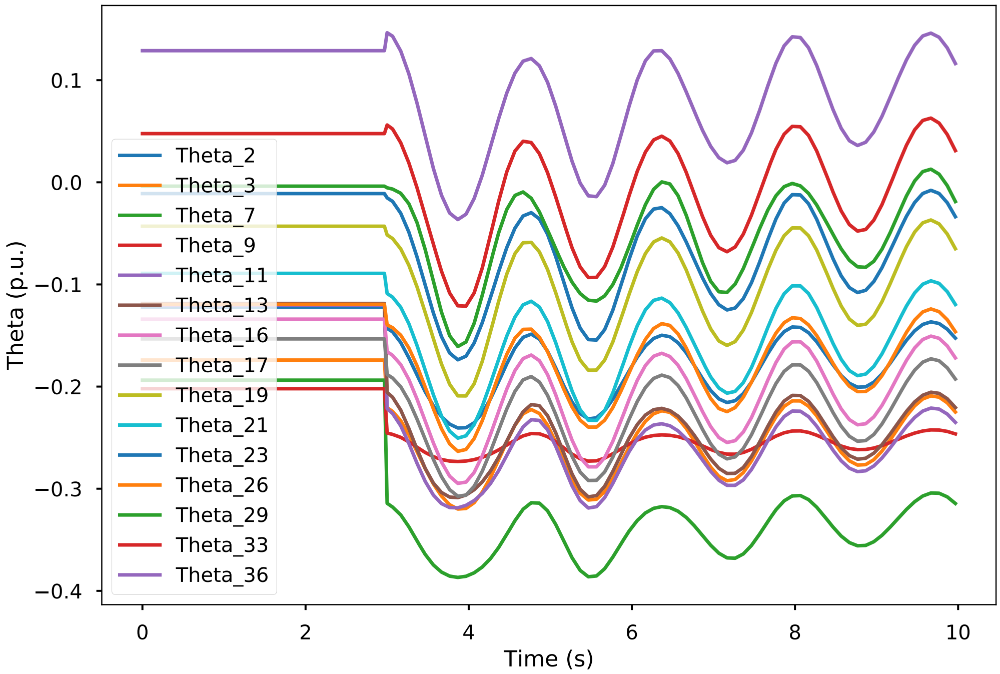

Figure 3.7: *The progression of bus voltage phase angles after the outage of line 37. Each line represents the voltage phase angles from one of the buses.*

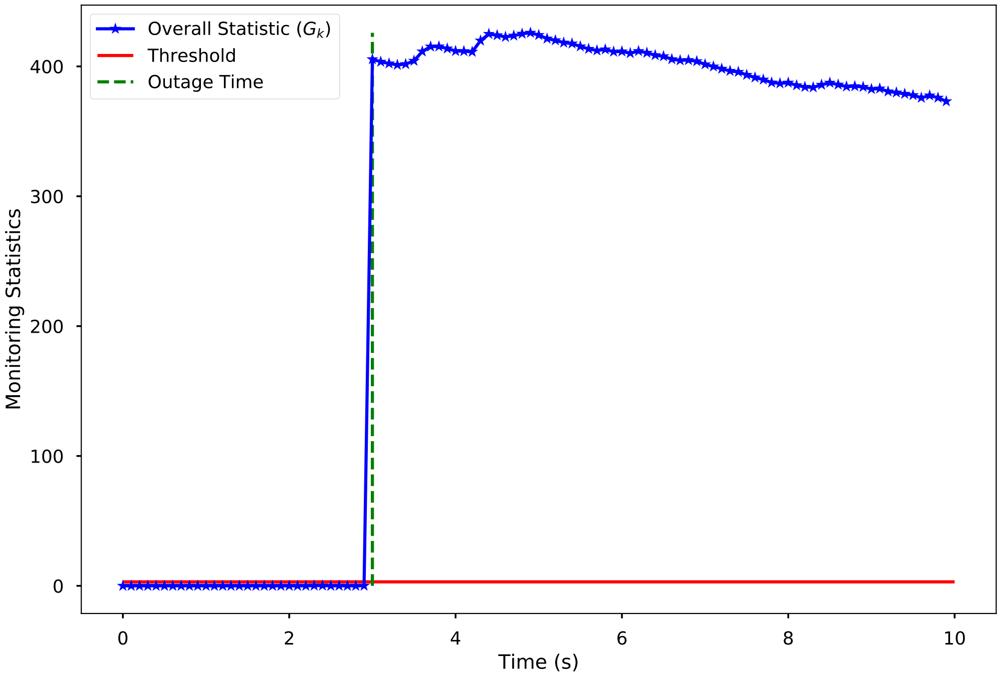

Figure 3.8: *The progression of the monitoring statistic for line 37 outage.*

Chapter 4

Outage Detection Using Generator Dynamics

The rest of this paper is organized as follows. A unified outage detection scheme based on nonlinear power system dynamics is formulated in Section 4.1. Section 4.2 then describes the PF-based online state estimation necessary for tracking generator dynamics. The proposed scheme's effectiveness and advantages are presented in Section 4.3 using simulation studies. Section 5.5 is the conclusion.

4.1 Problem Formulation

4.1.1 Power System Model

In this section, we detail a power system model that captures both the generator dynamics and load bus power flow information in a unified framework. Consider a power system with M generator buses where $\mathcal{N}_g = \{1, \dots, M\}$, $N - M$ load buses where $\mathcal{N}_l = \{M+1, \dots, N\}$, and L transmission lines where $\mathcal{L} = \{1, \dots, L\}$. Power system is a hybrid dynamical system described by a differential-algebraic model. The second-order generator model, also known as the swing equation [57], is used in this work[1]. For every generator bus $i \in \mathcal{N}_g$, their states are modeled as the differential variables, i.e., $\boldsymbol{X} = [\delta, \omega]^T$ where δ is the rotor angular position

[1] Although the swing equation is used here to model generator rotor dynamics, high-order and more complex models, such as the two-axis model [58], can be used. The detection scheme proposed in this work can be developed similarly.

in radians with respect to a synchronously rotating reference, and ω is the rotor angular velocity in radians/second. The differential equations governing their dynamics are

$$\dot{\delta}_i = \omega_s \left(\omega_i - 1\right) \,, \tag{4.1a}$$

$$M_i \dot{\omega}_i = P_{m,i} - \hat{P}_{g,i} - D_i \left(\omega_i - 1\right) \,, \tag{4.1b}$$

$\dot{\delta}_i$ is the derivative of δ_i with respect to t. ω_s is the synchronous rotor angular velocity such that $\omega_s = 2\pi f_0$ where f_0 is the known synchronous frequency. $P_{m,i}$, M_i, and D_i denote the mechanical power input, the inertia constant and the damping factor, respectively. They are assumed known and constant for the duration of our study. The inputs for the model are the generated active power, i.e., $u = P_g$. Under classical model assumptions, the synchronous machine is represented by a constant internal voltage $\mathrm{E}\angle\delta$ behind its direct axis transient reactance X_d' [57]. Therefore, the active power at generator i is

$$P_{g,i} = \frac{\mathrm{E}_i \mathrm{V}_i}{\mathrm{X}_{d,i}'} \sin(\delta_i - \theta_i) \,, \tag{4.2}$$

where θ is the generator bus nodal voltage phase angle. The transient reactance is assumed known and constant, whereas a method will be presented later to adaptively infer the parameter E with online data. Also, we denote $\hat{P}_{g,i} = P_{g,i} + \epsilon_i$ where ϵ is assumed to be a zero-mean Gaussian variable with a known variance representing the random fluctuations in electricity load on the bus as well as process noise.

The outputs of our system model are nodal voltage magnitudes and phase angles which PMUs can measure. More importantly, the algebraic output and generator states have to satisfy an active power balance constraint. The constraint stipulates that the net active power at a bus is the difference between the active power supplied to it by the generator and the load consumed, i.e.,

$$P_i = P_{g,i} - P_{l,i} \,, \tag{4.3}$$

for $i = 1, \dots, N$, subject to a random demand fluctuation ϵ_i as mentioned above. $P_{l,i}$ is the load on bus i, P_i is the nodal net active power and

$$P_i = \mathrm{V}_i \sum_{j=1}^{N} \mathrm{V}_j \mathrm{Y}_{ij} \cos(\theta_i - \theta_j - \alpha_{ij}) \,, \tag{4.4}$$

following the alternating current (AC) power flow equation where $\mathrm{Y}_{ij}\angle\alpha_{ij}$ are elements of the bus admittance matrix. Note that for load buses $P_{g,i} = 0$ in (4.3). The total active power generated and load demand of the network are assumed to be balanced as well. This relationship will be the basis for our unified outage detection scheme described in the next section.

We define the discrete counterparts of the system model via a first-order difference discretization by Euler's formula, i.e., let $\delta_{k+1} = \delta_(t_{k+1})$ for $k = 1, 2, \dots,$ and $\dot{\delta}_{t_{k+1}} \approx (\delta_{k+1} - \delta_k)/\Delta t$. For PMU devices with a sampling frequency of 30 Hz, $\Delta t = t_{k+1} - t_k = 1/30$ s. Thus, the continuous system of a generator bus i can be approximated by

$$\boldsymbol{X}_{i,k+1} = \begin{bmatrix} \delta_{i,k+1} \\ \omega_{i,k+1} \end{bmatrix} = \begin{bmatrix} \delta_{i,k} + \Delta t \omega_s \left(\omega_{i,k} - 1\right) \\ \omega_{i,k} + \frac{\Delta t}{M_i} q_{i,k} - \epsilon_k \end{bmatrix} \tag{4.5}$$

where $q_{i,k} = P_{m,i} - P_{g,i,k} - D_i\left(\omega_{i,k} - 1\right)$ for notational brevity, and

$$P_{g,i,k} = \frac{\mathrm{E}_i \mathrm{V}_{i,k}}{\mathrm{X}'_{d,i}} \sin(\delta_{i,k} - \theta_{i,k}) \,. \tag{4.6}$$

Taking a derivative with respect to time t on both sides of (4.3) and rearranging the terms, we obtain $\partial P_{l,i}/\partial t = \partial P_{g,i}/\partial t - \partial P/\partial t$, relating the changes in bus load to the changes in active power generated and transferred from the bus. The discretized relationship is then

$$\Delta P_{l,i,k} = \Delta P_{g,i,k} - \Delta P_{i,k} \,, \tag{4.7}$$

where $\Delta P_{l,i,k} = P_{l,i,k} - P_{l,i,k-1}$ and similarly for the other two terms. Writing the whole system in vector form, we also define

$$\boldsymbol{Y}_k = \Delta \boldsymbol{P}_{l,k} = \begin{bmatrix} \Delta \boldsymbol{P}_{g,k} \\ \boldsymbol{0} \end{bmatrix} - \Delta \boldsymbol{P}_k + \boldsymbol{\eta}_k \,, \tag{4.8}$$

where $\boldsymbol{\eta}$ represents the random load fluctuations and measurement error which we assume is a zero-mean Gaussian variable with covariance $\sigma^2\mathbf{I}$. The net active power change vector, i.e., $\Delta\boldsymbol{P}_k$, is organized such that the top M entries correspond to the M generator buses.

(4.8) allows us to monitor the active power changes in both generator and load buses. In comparison, detection schemes developed in previous works focus on monitoring changes in net active power, $\Delta\boldsymbol{P}$, through direct current (DC), e.g., [30], or AC, e.g., [16], power flow equations. Their formulations can be considered as the special cases of our unified framework when no generator information is available, e.g., no PMUs are installed on generator buses. However, as we show in simulation studies, having generator power output information helps to detect certain outages when net active power changes are not significant enough to trigger an alarm.

(4.5)-(4.8) define a state-space model (SSM) for the power system that could be summarized in the general form below:

$$\boldsymbol{X}_{k+1} = a(\boldsymbol{X}_k, \boldsymbol{u}_k, \boldsymbol{\epsilon}_k) \rightarrow f(\boldsymbol{X}_k|\boldsymbol{x}_{k-1}) \tag{4.9a}$$

$$\boldsymbol{Y}_k = b(\boldsymbol{X}_k, \boldsymbol{u}_k, \boldsymbol{\eta}_k) \rightarrow g(\boldsymbol{Y}_k|\boldsymbol{x}_k) \tag{4.9b}$$

In this SSM, the generator states $\boldsymbol{X}$ are not directly observable, and their dynamics are governed by the state transition function $a(\cdot)$ as in (4.5). The output $\boldsymbol{Y}$ can be computed from PMU measurements as well as generator states and is governed by the output function $b(\cdot)$ as in (4.8). Note that $b(\cdot)$ is a nonlinear function of the system states; therefore, the power system is a nonlinear dynamical system. As the process is stochastic due to random load fluctuations and measurement errors, we can express the states and output in a probabilistic way. In particular, we denote the state transition density and output density as $f(\boldsymbol{X}_k|\boldsymbol{X}_{k-1} = \boldsymbol{x}_{k-1})$ and $g(\boldsymbol{Y}_k|\boldsymbol{X}_k = \boldsymbol{x}_k)$, respectively, where $f(\cdot)$ and $g(\cdot)$ are probability density functions (PDFs). An important consequence of the SSM is the conditional independence of the states and output due to the Markovian structure. In particular, given $\boldsymbol{X}_{k-1}$, $\boldsymbol{X}_k$ is independent of all other previous states; similarly given $\boldsymbol{X}_k$, $\boldsymbol{Y}_k$ is independent of all other previous states.

4.1.2 Outage Detection Scheme

We propose a system-wide detection scheme that utilizes the output of the SSM detailed in the previous section. Under an outage-free scenario, we expect the active power generated, transmitted, and consumed in the network are balanced with only small random load demand fluctuations. Therefore, the distribution of the system output is the basis for our outage detection scheme:

$$\boldsymbol{Y}_k = \begin{bmatrix} \Delta \boldsymbol{P}_{g,k} \\ \boldsymbol{0} \end{bmatrix} - \Delta \boldsymbol{P}_k + \boldsymbol{\eta}_k \sim N(\boldsymbol{0}, \sigma^2 \boldsymbol{I})\,. \tag{4.10}$$

When a line trips in the power grid, there are two ways that the above relationship will be violated. First, the system topology changes, therefore the outage-free AC power flow equation (4.4) used to compute the net active power is no longer valid[2]. Thus $\Delta \boldsymbol{P}$ in (4.10) does not represent the actual net active power changes anymore. Second, line outage events trigger a period of transient re-balancing in the system where generators respond to the power imbalance caused by the outage. The immediately affected buses also experience an abrupt change in the net active power due to the outage. As a combination of these effects, the relationship of (4.10) will be violated. For example, using data simulated from the IEEE 39-bus test system, Fig. 4.1 shows the contrast between the signals from a normal system and that with an outage at the 3rd second.

Therefore, we have formulated the early outage detection problem as a multivariate process monitoring problem. The multivariate signal's deviation, $\Delta \boldsymbol{Y}$, from the expected distribution indicates an abnormal event, in this case, an outage. For its robustness to non-Gaussian data and superior performance on small to median shifts, we adopt the multivariate exponentially weighted moving average (MEWMA) control chart, initially developed by [59], for the detection task. In particular, with system outputs computed from PMU measurements and estimated generator states, $\boldsymbol{y}_k$, we

[2]In particular, the admittance corresponding to the tripped line becomes zero, and the bus admittance matrix Y changes to a new one that reflects the post-outage system topology.

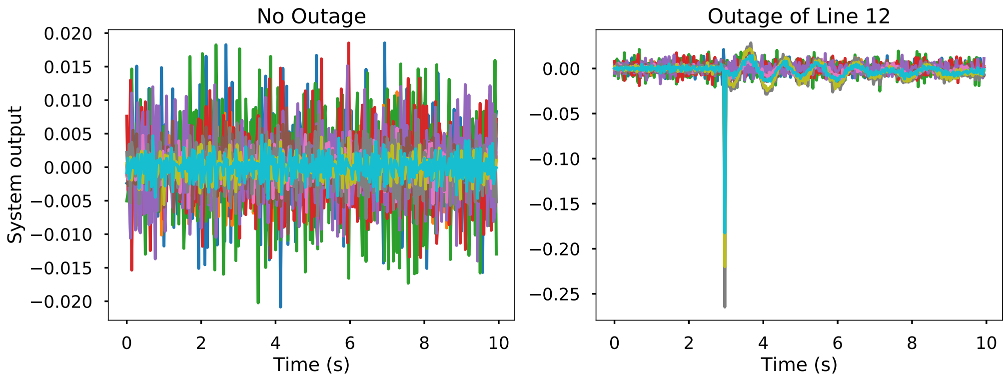

Figure 4.1: Comparison of the output signals with no outage and with line 12 outage. A subset of output signals significantly deviated from the normal mean level and exhibited strong non-Gaussian oscillations.

construct an intermediate quantity that captures not only current but also past signal information, i.e.,

$$\boldsymbol{Z}_i = \lambda \boldsymbol{y}_k + (1-\lambda)\boldsymbol{Z}_{i-1}\,, \tag{4.11}$$

where λ is a pre-defined smoothing parameter that determines the extent of reliance on past-information and $0 < \lambda \leq 1$, $\boldsymbol{Z}_0 = \boldsymbol{0}$. The statistic under monitoring is then constructed similiar to that of a Hotelling T^2 statistic:

$$T_k^2 = \boldsymbol{Z}_k^T \Sigma_{\boldsymbol{Z}_k}^{-1} \boldsymbol{Z}_k\,, \tag{4.12}$$

where the covariance matrix is

$$\Sigma_{\boldsymbol{Z}_k} = \frac{\lambda}{2-\lambda}\left[1-(1-\lambda)^{2k}\right]\sigma^2\,.$$

An outage alarm is then triggered when the monitoring statistic crosses a pre-determined threshold, H, chosen to satisfy a certain sensitivity requirement:

$$D = \inf\{k \geq 1 : T_k^2 \geq H\}\,. \tag{4.13}$$

Here D is the stopping time of our outage detection scheme. The difference between D and the onset time of the outage is the detection delay. Our detection scheme's prime objective is to minimize the detection delay should an outage happen at an a priori unknown location.

A common way to quantify the detection scheme's sensitivity is through the so-called average run length to a false alarm (ARL_0), i.e., the number of samples required to produce a false alarm when the system is outage-free. MEWMA-type control chart allows system operators to specify an appropriate sensitivity level by selecting λ and H. Charts with lower values of λ are generally more robust against non-Gaussian distributions and have better detection performance for small to medium shifts [56]. Given λ and a false alarm constraint ARL_0, the detection threshold H can be determined by solving an integral equation of Theorem 2 in [60][3]. The selection of the parameter values and their impact on the detection scheme will be presented in the case studies section.

4.2 Generator State Estimation

In the previous section, we have described a unified framework of real-time system monitoring utilizing post-outage transient dynamics computed from state and algebraic variables, i.e., active power generated and net active power injection. The premise of the unified framework is the availability of accurate state and algebraic variables data. While algebraic variables can be measured by PMUs, generator states are not directly observable. This section shows how the hidden states could be reliably estimated online using a particle filter.

Online state estimation typically involves the inference of the posterior distribution of the hidden states $\boldsymbol{X}_k$ given a collection of output measurements $\boldsymbol{y}_{0:k}$, which we denoted by $\pi(\boldsymbol{X}_k|\boldsymbol{y}_{0:k})$. For systems with nonlinear dynamics and possibly non-Gaussian noises, e.g., power system, the posterior distribution is intractable and cannot be computed in closed form. To solve the above problem, extended and unscented Kalman filter have been extensively studied, e.g., [62, 63]. However, the above methods' effectiveness becomes questionable when the underlying nonlinearity is substantial

[3]The equation can be solved using various numerical algorithms or Markov chain approximation, and this process can be done offline. We refer interested readers to [61] for a detailed description of the computation procedure required.

or when the posterior distribution is not well-approximated by Gaussian distribution. Instead, PF is increasingly used for this task, e.g., [64], as it handles nonlinearity well and accommodates noise of any distribution with an affordable computational cost [65, 66]. PFs belong to the family of sequential Monte Carlo methods where Monte Carlo samples approximate complex posterior distributions, and the distribution information is preserved beyond mean and covariance.

In particular, PF approximates $\pi(\boldsymbol{X}_k|\boldsymbol{y}_{0:k})$ by samples, called particles, obtained via an importance sampling procedure. Each particle is assigned an importance weight proportional to its likelihood of being sampled from the posterior distribution[4]. PF proceeds in a recursive prediction-correction framework. Assuming at time k we have the particles and weights obtained from the previous time step, $\{(\boldsymbol{x}_{k-1}^i, w_{k-1}^i)\}_{1\leq i\leq N_p}$, where N_p is the number of particles, the posterior distribution at time $k-1$ is approximated by weighted Dirac delta functions as

$$\pi(\boldsymbol{X}_{k-1}|\boldsymbol{y}_{0:k-1}) \approx \sum_{i=1}^{N_p} w_{k-1}^i \cdot \delta(\boldsymbol{X}_{k-1} - \boldsymbol{x}_{k-1}^i)\,, \tag{4.14}$$

where $\delta(\cdot)$ is the Dirac delta function, and the weights are normalized such that $\sum_{i=1}^{N_p} w_{k-1}^i = 1$. The algorithm starts by propagating particles from time $k-1$ to time k through the state transition function in (4.5), i.e., the prediction step. That means, new particles $\{\boldsymbol{x}_k^i\}_{1\leq i\leq N_p}$ are sampled from the state transition density $f(\boldsymbol{X}_k|\boldsymbol{x}_{k-1}^i)$. The predicted states then have a prior distribution approximated by

$$\pi(\boldsymbol{X}_k|\boldsymbol{Y}_{0:k-1}) \approx \sum_{i=1}^{N_p} w_{k-1}^i \cdot \delta(\boldsymbol{X}_k - \boldsymbol{x}_k^i)\,. \tag{4.15}$$

When the new measurement y_k arrives, the prior distribution is corrected by updating the particles' weights proportional to their conditional output

[4]This type of PF is also known as the bootstrap filter first proposed in [67]. The idea is to use the state transition density as the importance distribution in the importance sampling step. More sophisticated algorithms, such as the guided and auxiliary particle filter could be implemented in the same detection framework proposed here. However, these algorithms are, in general, more difficult to use and interpret. For details, readers can refer to [68].

likelihood to obtain the posterior distribution as

$$\pi(\boldsymbol{X}_k|\boldsymbol{Y}_{0:k}) \approx \sum_{i=1}^{N_p} w_k^i \cdot \delta(\boldsymbol{X}_k - \boldsymbol{x}_k^i)\,, \tag{4.16}$$

where $w_k^i \propto w_{k-1}^i \cdot g(\boldsymbol{y}_k|\boldsymbol{x}_k^i)$. The intuitive interpretation is that the particles are reweighted based on their compatibility with the actual system measurement. The approximation of the posterior distribution by these particle-weight pairs is consistent as $N_p \to +\infty$ at a standard Monte Carlo rate of $\mathcal{O}(N_p^{-1/2})$ guaranteed by the Central Limit Theorem [68].

A well-known problem of PF is that the weights will become highly degenerate overtime. In particular, the density approximation will be concentrated on a few particles, and all the other particles carry effectively zero weight. A common way to evaluate the extent of this degeneracy is by using the so-called Effective Sample Size (ESS) criterion [69]:

$$\mathrm{ESS} = \left(\sum_{i=1}^{N_p} \left(w_k^i\right)^2\right)^{-1} . \tag{4.17}$$

In the extreme case where one particle has the weight of 1 and all others of 0, ESS will be 1. On the other hand, ESS is N_p when every particles has an equal weight of N_p^{-1}. A resampling move can be used to solve the degeneracy problem where particles with higher weights are duplicated and others removed, thus focusing computational efforts on regions of higher probability. The systematic resampling method is used in our PF as it usually outperforms other resampling algorithms [68]. When ESS falls below a threshold, typically $N_p/2$, we resample N_p particles from the existing ones. The number of offsprings, N_k^i, is assigned to each particle $\boldsymbol{x}_k^i$ such that $\sum_{i=1}^{N_p} N_k^i = N_p$. The systematic sampling proceeds as follows to select N_k^i. A random number U_1 is drawn from the uniform distribution $\mathcal{U}\left[0, {N_p}^{-1}\right]$. Then we obtain a series of ordered numbers by $U_i = U_1 + \frac{i-1}{N_p}$ for $i = 2, \ldots, N_p$. N_k^i is the number of $U_i \in (\sum_{s=1}^{i-1} w_s, \sum_{s=1}^{i} w_s]$ where $\sum_{s=1}^{0} w_s := 0$ by convention. Finally, resampled particles are each assigned an equal weight N_p^{-1} before a new round of prediction-correction recursion begins. The detailed PF algorithm with the resampling move is summarized in Algorithm 1.

Algorithm 1 Particle Filter

for $i = 1, \ldots, N_p$ **do** ▷ Initialization
    Sample $\tilde{\boldsymbol{x}}_0^i \sim \pi_0(\boldsymbol{X})$.
    Compute initial importance weight $\tilde{w}_0^i = g(\boldsymbol{y}_0 | \tilde{\boldsymbol{x}}_0^i)$.
end for
for $k \geq 1$ **do**
    if ESS $\leq N_p/2$ **then** ▷ Systematic resampling
        Draw $U_1 \sim \mathcal{U}\left[0, {N_p}^{-1}\right]$ and obtain $U_i = U_1 + \frac{i-1}{N_p}$ for $i = 2, \ldots, N_p$.
        for $i = 1, \ldots, N_p$ **do**
            Obtain N_k^i as the number of U_i such that

$$U_i \in \left(\sum_{s=1}^{i-1} w_s, \sum_{s=1}^{i} w_s \right] .$$

            Select N_p particle indices $j_i \in \{1, \ldots, N_p\}$ according to N_k^i.
            Set $\boldsymbol{x}_{k-1}^i = \tilde{\boldsymbol{x}}_{k-1}^{j_i}$, and $w_{k-1}^i = 1/N_p$.
        end for
    else
        Set $\boldsymbol{x}_{k-1}^i = \tilde{\boldsymbol{x}}_{k-1}^i$ for $i = 1, \ldots, N_p$.
    end if
    for $i = 1, \ldots, N_p$ **do**
        Propagate particles ▷ Prediction

$$\tilde{\boldsymbol{x}}_k^i \sim f(\boldsymbol{X}_k | \boldsymbol{x}_{k-1}^i) .$$

        Update weight ▷ Correction

$$\tilde{w}_k^i = w_k^i \times g(\boldsymbol{y}_k | \tilde{\boldsymbol{x}}_k^i) .$$

    end for
    Normalize weights

$$w_k^i = \frac{\tilde{w}_k^i}{\sum_{k=1}^{N_p} \tilde{w}_k^k} \text{, for } i = 1, \ldots, N_p .$$

end for

4.2.1 Additional Remarks

Limited PMU Deployment Many power systems have to work with a limited number of PMUs, i.e., some buses are not equipped with a PMU. The detection scheme proposed here is also applicable in this case since the signal under monitoring, $\boldsymbol{Y}$, can be adjusted to include only buses with PMUs. In particular, $\Delta \boldsymbol{P}_g$ can include those generator buses with PMUs. $\Delta \boldsymbol{P}$ can be calculated for load buses with fully observable neighbor buses. The impact of an unobservable neighbor bus on the computation of the bus net active power would be an unknown term, $\mathrm{V}_j \mathrm{Y}_{ij} \cos(\theta_i - \theta_j - \alpha_{ij})$, in the AC power flow equation since the neighbor bus' θ_j and V_j are not available. While this impact can be mitigated through a careful selection of the PMU locations, unlike [30] and [16], the proposed detection scheme is effective when most generator buses are monitored, a result corroborated by our simulation study, e.g., see Fig. 4.6. Also, the number of generator buses is typically much smaller than the total number of buses.

Unknown System Parameter Estimation We have assumed that the system parameters in the power system SSM are known and static; therefore, the PF's state estimation is reliable. In real-world applications, these parameters may be known but slow-varying due to factors like system degradation. While parameter estimation in a non-linear system is generally a difficult problem and outside the scope of this paper, there is a natural extension from the particle filtering framework that can tackle the problem. An online expectation maximization (EM) algorithm based on the particles can be implemented to learn the parameters as data arrives sequentially in real-time. The EM algorithm is an iterative optimization method that finds the maximum likelihood estimates of the parameters in problems where hidden variables are present[70]. This basic EM algorithm can be reformulated to perform the estimation online using the so-called sequential Monte Carlo forward smoothing framework when the complete-data density, i.e., $p_\vartheta(\boldsymbol{x}_{0:k}, \boldsymbol{y}_{0:k})$ where ϑ denote the set of unknown parameters, is from the exponential family [71].

4.3 Simulation Study

4.3.1 Simulation Setting

The proposed PF-based outage detection scheme is tested on the IEEE 39-bus 10-machine New England system[53]. System transient responses after an outage are simulated using the open-source dynamic simulation platform COSMIC [54]. A third-order machine model and AC power flow equations are used. We assume that the simulation results are the true generator states, and corrupted measurements are synthesized from the noise-free simulation data. For PMUs, we assume ten are installed at bus 19, 20, 22, 23, 25, 33, 34, 35, 36, and 37, covering five generator buses and their connected load buses. We also assume their sampling frequency is 30 samples per second. Each simulation runs for 10 seconds, and the outage happens at the 3rd second. A line outage is detected if the monitoring statistic crosses the detection threshold by the end of the simulation. The global constants are $f_0 = 60$ Hz and $\omega_s = 1.0$ p.u.. For our SSM, state function noise ϵ_k are assumed to be uncorrelated and homogeneous with a standard deviation of $0.01\% \cdot \mathrm{P}_{g,k}$ in (4.5). Output function error $\boldsymbol{\eta}_k$ are assumed to follow a zero-mean Gaussian distribution with a standard deviation of $1\% \cdot (\mathrm{P}_{g,k} - \mathrm{P}_k)$ in (4.8).

4.3.2 Illustrative Outage Detection Example

To illustrate the working of the detection scheme, we use line 18 outage as an example. Fig. 4.2 shows a typical performance of the particle filter used to estimate generator states. The rotor angular speed, ω, can be accurately tracked while the rotor angular position, δ, has some biases after the outage. This is acceptable since we are more concerned with capturing the abnormal changes, i.e., $\Delta\delta$ and in turn ΔP_g, in response to the outage rather than accurate state estimations.

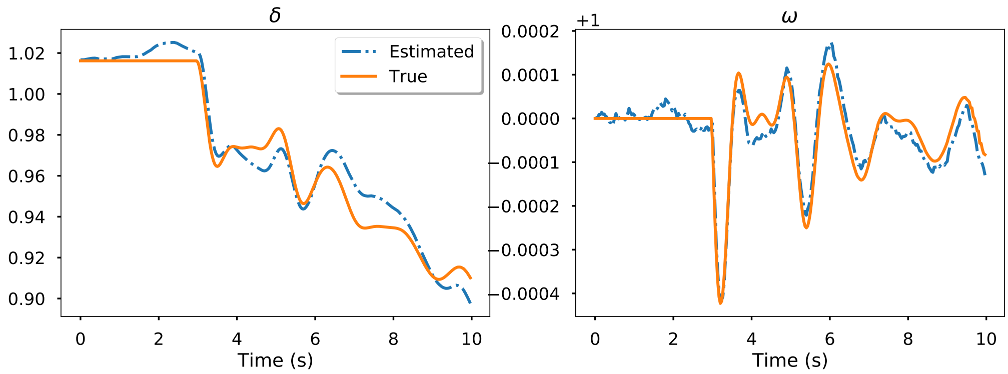

Figure 4.2: State estimation result of the particle filter on δ and ω of Bus 33. The algorithm can estimate ω accurately, while the estimation of δ has biases after the outage. The changes in δ are sufficiently captured, which are more critical for the detection scheme.

One significant advantage of the proposed detection scheme is the ability to break down the output signals and pinpoint the components leading to early detection. Fig. 4.3 shows such a breakdown for line 18 outage. The upper two components are the generator bus information, and the lower-left one is the load bus information. They register different signal strength levels depending on the outage location, e.g., the magnitude of initial shock, the magnitude, and the transient oscillation duration. Our scheme can detect outages as long as one of them picks up significant changes. It is clear in this case that the signals from monitored load buses do not contribute meaningfully to the outage detection. Instead, the changes in generated active power and net power injection on generator buses display significant abnormal fluctuations, leading to the outage detection. The typical progression of the monitoring statistic, T_k^2, computed via MEWMA from the output signals is shown in Fig. 4.4. Before the outage, the statistic remains close to zero. After the outage at the 3rd second, it increases rapidly and crosses the threshold. Thus, the scheme raises an outage alarm, and no detection delay is incurred.

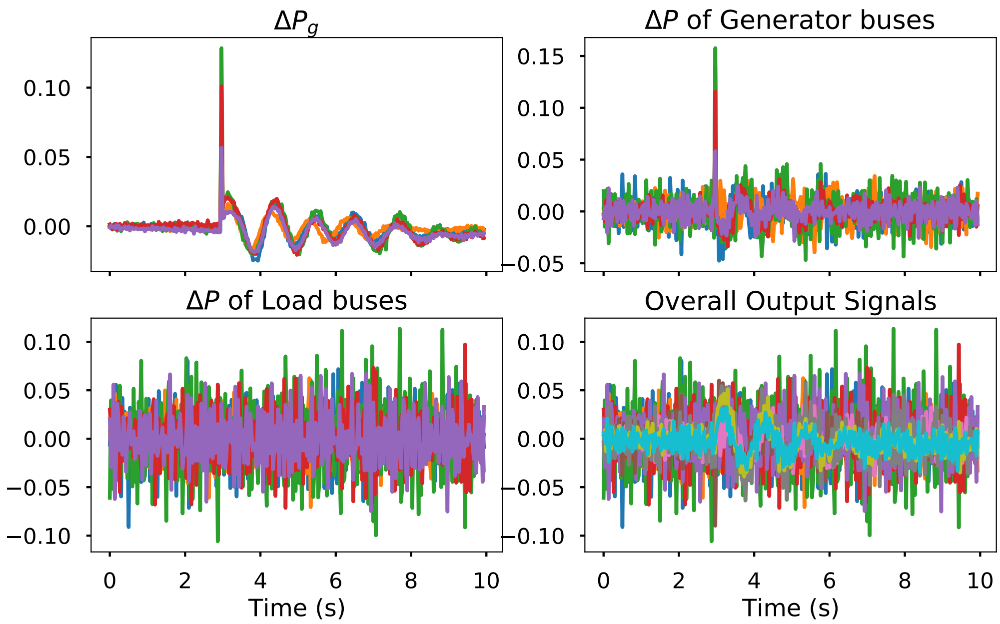

Figure 4.3: Output signals of the detection scheme for line 18 outage and its breakdown by components. Each line in the figure represents data from a bus equipped with a PMU. Abnormal disturbances in generator rather than load buses contributed to early detection in this case.

4.3.3 Results and Discussion

This section shows the effectiveness of the proposed unified scheme using average performance computed from 1000 random simulations of each line outage. We also present a performance comparison with other state-of-the-art methods.

Detection Rate Fig. 4.5 presents the empirical likelihood of detection for all 35 simulated line outages, which is the percentage of successful detections over 1000 simulations. For both small and large values of λ, the detection scheme can detect 28 out of 35 outages over 90% of the time. In some cases, we see that larger values of λ tend to have a better detection rate, i.e., line 8, 13, 15, and 26. The reason is that these line outages produce more severe initial shock relative to their after-outage oscillation. Hence, larger values of λ help to capture the immediate shock. Also, a small group of outages is

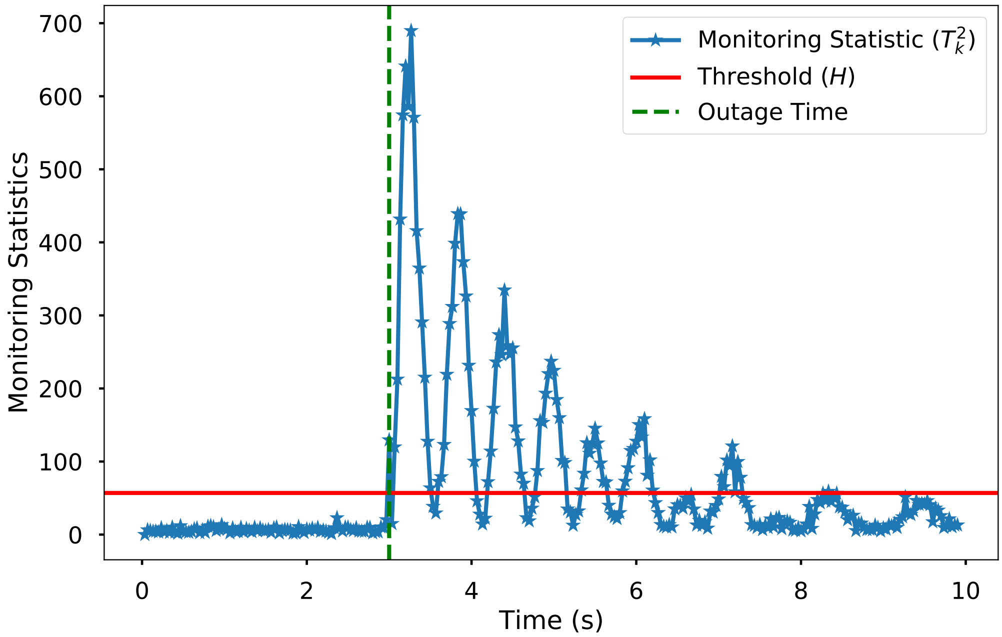

Figure 4.4: Progression of MEWMA monitoring statistic for detecting line 18 outage. After the outage onset, the monitoring statistic crosses the detection threshold immediately and remains high afterward. The outage is successfully detected with no detection delay.

challenging to detect regardless of the λ value, i.e., line 2, 6, 19, 35, and 36. Diagnostic inspection of these cases' output signals reveals that they generally produce weak system disturbances, especially from the generators, hence often not triggering an outage alarm. The weak disturbance might be explained by the fact that these lines are connected to buses that serve zero or small loads.

Detection Delay The empirical distribution of the detection delays is presented in Fig. 4.6. The figure shows the results of the proposed scheme with different λ values and the detection scheme based on AC power flow equations from [16]. Intuitively, the scheme is faster at detecting outages when the area under the curve towards the left of the figure is larger. In this case, the proposed scheme has a much higher chance of detecting outages with zero detection delay than the AC scheme. The best-performing scheme

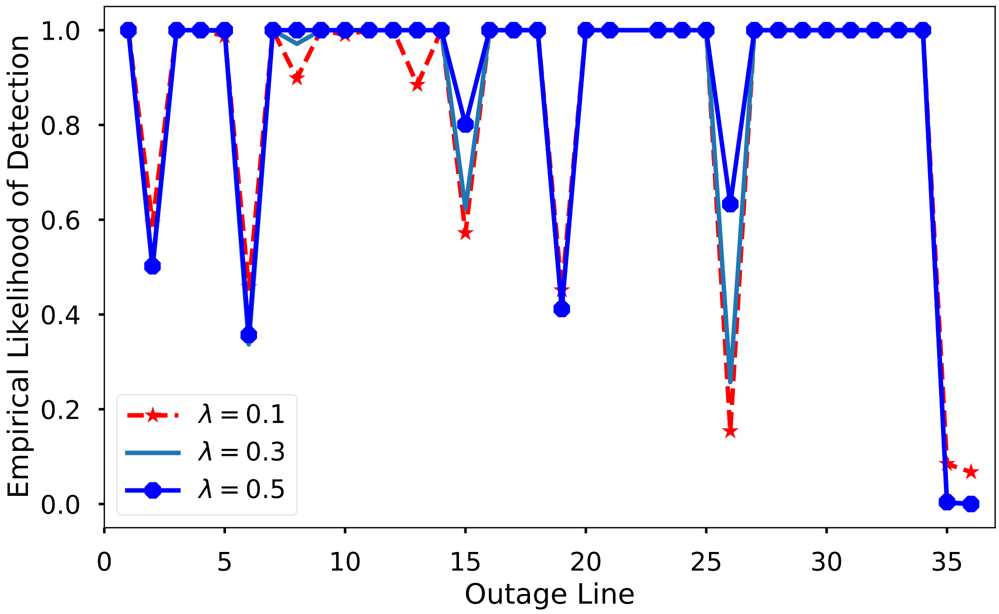

Figure 4.5: Comparison of the empirical likelihood of detection for all simulated outages under different λs of MEWMA. While 28 out of the 35 line outages can be detected with over 90% likelihood, larger values of λ tend to have a higher detection rate. A small group of outages is difficult to detect regardless of the λ value.

($\lambda = 0.5$) also detects most outages within 0.2 seconds, whereas the AC scheme detects most outages within 1 second.

Effect of Outage Location Relative to the PMUs In some related and our previous studies, we observed significant variations of average detection delays for outages at different lines relative to the PMU locations. Fig. 4.7 shows a comparison of detection delays for outage lines with at least one PMU connected to it versus those with no PMU nearby. Since only ten buses are equipped with PMUs, most lines belong to the second group[5]. While outages at line 11 and 19 are often detected with 0.1-second delay, most outages are detected immediately regardless of the relative position

[5]Only a few lines in the second group are presented due to space constraints. All of those omitted line outages can be detected with zero mean detection delay, except for line 35, and 36, which are often undetected.

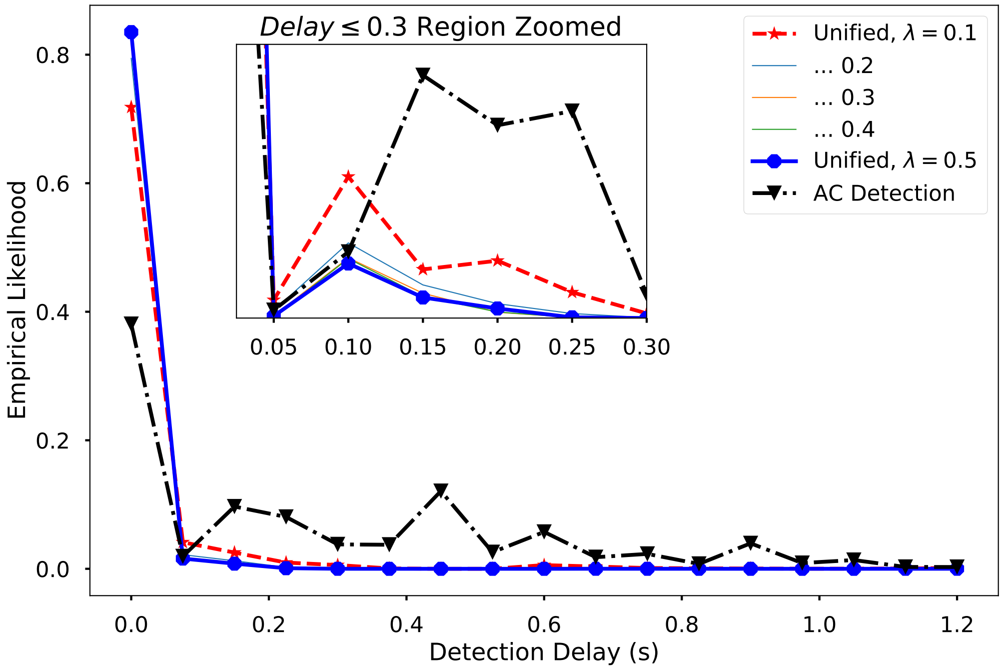

Figure 4.6: Comparison of the empirical distribution of detection delays in seconds for the proposed unified scheme and the scheme based on AC power flow equations. The proposed scheme has a higher percentage of zero detection delays. It can detect almost all outages within 0.2 seconds, whereas the AC detection scheme does it in 1 second.

to the PMUs. Line 11 connects to the slack bus, and its outage creates a minimal disturbance in all three output channels. This result demonstrates the spatial advantage of the proposed method and its robustness to the outage locations.

Comparison with Other Methods We compare the proposed method's performance with three other methods in Table 4.1. The chosen outages are, in general, more difficult to detect. The first method for comparison is based on the DC power flow model from [30] and the second based on subspace identification from [22]. Both of them are tested using a full PMU deployment. The third is from our previous work that relies on the AC power flow model where 10 PMUs are assumed to be installed at locations used in [16]. The thresholds for all methods are selected by satisfying a

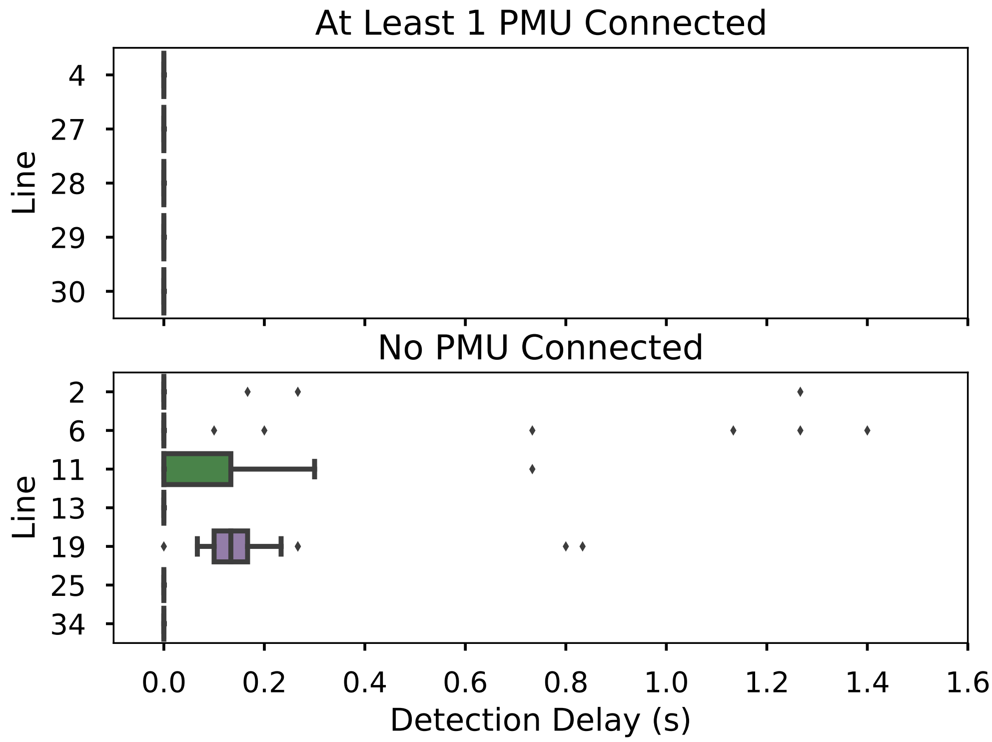

Figure 4.7: Box plot of the empirical distributions of detection delays in seconds for lines with at least 1 PMU nearby and those without a PMU.

Table 4.1: Detection Delay Comparison of Different Detection Schemes

	Average Detection Delay (s.d.)			
Line	DC (full)	Subspace (full)	AC	Unified
2	1.165 (0.006)	2.822 (1.924)	0.283 (0.263)	**0.012** (0.183)
6	–	3.060 (2.011)	0.246 (0.129)	**0.052** (0.463)
11	**0** (0)	3.048 (1.969)	0.602 (0.205)	0.058 (0.077)
15	**0** (0)	2.634 (1.850)	0.005 (0.034)	**0** (0)
19	–	2.836 (2.018)	0.335 (0.378)	**0.160** (0.315)
26	–	2.850 (1.958)	0.385 (0.228)	**0** (0)

false alarm constraint of 1 in 30 days. The average detection delays and their standard deviations are computed from 1000 random simulations, while a dash means a missed detection. The method proposed, “Unified”, is consistently faster at detecting outages than the other methods.

4.4 Conclusion

We have proposed a unified framework of online transmission line outage detection utilizing information from both generator machine states and load bus algebraic variables. The signals are obtained through nonlinear state estimation of particle filters and direct measurements of PMUs. They are effectively used for outage monitoring and detection by MEWMA control charts while meeting a particular false alarm criterion. The approach is shown to be quicker at detecting outages and more robust to a priori unknown outage locations under a limited PMU deployment through an extensive simulation study. Further research can be done to improve the detection scheme's effectiveness by investigating the optimal location of limited PMUs given a network of power stations. Also, we observed a group of lines that are consistently difficult to detect regardless of the detection schemes or parameter designs used. More work needs to be done in this area so that detection blind spots could be significantly reduced.

Chapter 5

Multiple-line Outage Identification

5.1 Introduction

Our contributions can be summarized in three aspects: 1) We improve the state-of-the-art multiple-line outage identification performance under limited PMU deployment; 2) The novel sparse regression formulation accommodates unknown number of outage lines and is robust with noisy data; 3) We also propose a way to account for indistinguishable outages using minimal diagnosable clusters which significantly improve overall identification accuracy.

The rest of this paper is organized as follows. The basis for outage identification is the post-outage voltage angle signature and is derived in Section 5.2. Multiple-line outage identification scheme is then described in Section 5.3. Section 5.4 demonstrates the effectiveness of the proposed scheme compared to existing ones. We conclude this work and discuss future research directions in Section 5.5.

5.2 Phase Angle Signature of Outages

Each outage is different. Machine learning-based approaches let algorithms learn the difference through clever training and generalizable data.

Physics-informed approaches, e.g., our proposed method, leverage physical laws governing power systems to find out the difference instead. In general, two questions need to be answered to build an effective physics-informed outage identification scheme: 1) How to quantify the impact of each line outage to nodal bus state variables? 2) Given the characterization, how to identify the most probable outage lines out of all possible ones? We explain in this section how the first question can be answered through sensitive analysis on AC power flow model. In the next section, an efficient and robust identification scheme is developed.

5.2.1 Power Flow Model

Consider a power system with N buses and L transmission lines where $\mathcal{N} = \{1, 2, \dots, N\}$ and $\mathcal{L} = \{1, 2, \dots, L\}$. AC power flow model is the governing equation between active and reactive power injection (P, Q) and voltage phasor ($\mathrm{V}\angle\theta$) at each bus [34]:

$$\mathrm{P}_m = \mathrm{V}_m \sum_{n=1}^{N} \mathrm{V}_n \mathrm{Y}_{mn} \cos(\theta_m - \theta_n - \alpha_{mn}) \,, \tag{5.1a}$$

$$\mathrm{Q}_m = \mathrm{V}_m \sum_{n=1}^{N} \mathrm{V}_n \mathrm{Y}_{mn} \sin(\theta_m - \theta_n - \alpha_{mn}) \,, \tag{5.1b}$$

where $m \in \mathcal{N}$, and $\boldsymbol{Y}$, the bus admittance matrix of which $\mathrm{Y}_{mn}\angle\alpha_{mn}$ is the $(m,n)_{th}$ element, is assumed to be known. V_m and θ_m are also assumed to be available if bus m has a PMU. Let $\mathbf{P}$, $\mathbf{Q}$, $\boldsymbol{\theta}$, and $\mathbf{V}$ represent the N-vectors of active and reactive power injection, voltage angles, and magnitudes at all buses except the reference bus[1]. A sensitivity analysis on power injections by linearization of (5.1a) around a pre-outage steady-state operating point yields the following partial differential equation:

$$\Delta\mathbf{P} \approx J_1 \Delta\boldsymbol{\theta} + J_2 \Delta\mathbf{V} \,, \tag{5.2}$$

where J_1, J_2 are two submatrices of the AC power flow Jacobian with

$$J_1 = \frac{\partial \mathbf{P}}{\partial \boldsymbol{\theta}} \,, J_2 = \frac{\partial \mathbf{P}}{\partial \mathbf{V}} \,. \tag{5.3}$$

[1]By convention, bus 1 is assumed to be the reference bus whose voltage phase angle is set to 0° and magnitude to 1.0 per unit (p.u.).

We let $\Delta\mathbf{P} = \mathbf{P}' - \mathbf{P}$ where $\mathbf{P}$ and $\mathbf{P}'$ denote pre- and post-outage bus power injections. $\Delta\boldsymbol{\theta} = \boldsymbol{\theta}' - \boldsymbol{\theta}$ is similarly defined. In the usual operating range of relatively small angles, power systems exhibit much stronger interdependence between $\mathbf{P}$ and $\boldsymbol{\theta}$ as compared to $\mathbf{P}$ and $\mathbf{V}$ [46]. Therefore, we focus on the relationship between real power injection and voltage phase angle, i.e., J_1, in the remainder of the paper[2]. Redefining J_1 as J, the off-diagonal and diagonal elements of J can be derived from (5.1a) as:

$$\frac{\partial \mathrm{P}_m}{\partial \theta_n} = \mathrm{V}_m \mathrm{V}_n \mathrm{Y}_{mn} \sin\left(\theta_m - \theta_n - \alpha_{mn}\right) \, , m \neq n \, , \tag{5.4a}$$

$$\frac{\partial \mathrm{P}_m}{\partial \theta_m} = - \sum_{\substack{n=1 \\ n \neq m}}^{N} \mathrm{V}_m \mathrm{V}_n \mathrm{Y}_{mn} \sin\left(\theta_m - \theta_n - \alpha_{mn}\right) \, . \tag{5.4b}$$

5.2.2 Outage Signature Map

We established an AC power flow-based relationship between instantaneous real power injection changes and voltage phase angle changes as $\Delta\mathbf{P} = J\Delta\boldsymbol{\theta}$. Inverting the Jacobian matrix, the relationship can be written as:

$$\Delta\boldsymbol{\theta} = J^{-1}\Delta\mathbf{P} \, . \tag{5.5}$$

Therefore, J^{-1} in (5.5) quantifies the impact on bus angles associated with respect to a unit change in real power injections. Under the DC assumption, a neat way to characterize the impact of an outage at line l carrying power from bus i to j is a real power injection of p_l at bus i and withdrawal of $-p_l$ at bus j [72]. Equivalently, the change in real power injection due to an outage at line l can be written as:

$$\Delta\mathbf{P} = p_l \cdot m_l \, .$$

m_l is an N-vector of zeros except with 1 at the i_{th} and -1 at the j_{th} position. p_l is a constant that depends on the pre-outage power flow and the

[2] The same set of analysis can applied to reactive power and voltage magnitude as well, which we omit here. We also skip some details about power system linearization as the formulation is standard. Interested reader can refer to Section II of [16].

so-called power transfer distribution factor [73]. In general, we can obtain the expected change in phase angles due to all outages at line $l_i, i \in \mathcal{L}$. Putting the p_l and m_l for all transmission lines together and write in matrix form:

$$\begin{aligned}[][\Delta\boldsymbol{\theta}] &= J^{-1}\begin{bmatrix} p_{l_1}m_{l_1} & p_{l_2}m_{l_2} & \cdots & p_{l_L}m_{l_L}\end{bmatrix} \\ &= J^{-1}\begin{bmatrix} m_{l_1} & m_{l_2} & \cdots & m_{l_L}\end{bmatrix}\operatorname{diag}(\boldsymbol{p}) \\ &= J^{-1}M\operatorname{diag}(\boldsymbol{p})\,, \end{aligned} \tag{5.6}$$

where M is the $N \times L$ bus to branch incidence matrix with columns corresponding to lines and rows to buses. $\operatorname{diag}(\boldsymbol{p})$ is the diagonal matrix with individual line power transfer p_l on the diagonal. M encodes the baseline system topology information, i.e., which bus is connected by which group of lines. It is also closely related to the bus admittance matrix $\boldsymbol{Y}$ since

$$\boldsymbol{Y} = M\operatorname{diag}(\mathbf{y})M^\top\,, \tag{5.7}$$

where $M^\top$ is the transpose of M and $\mathbf{y}$ is the vector of individual line admittance.

In a realistic setting of limited PMU deployment, we assume there are fewer PMUs than buses and transmission lines, i.e. $K \leq N$ and $K \leq L$. Define a bus selection matrix $S \in \{0,1\}^{K\times N}$ that selects rows of buses with PMUs, the observable phase angle impact from all line outages is

$$\begin{aligned}[][\Delta\boldsymbol{\theta}]_I &= SJ^{-1}M\operatorname{diag}(\boldsymbol{p}) \\ &= F\operatorname{diag}(\boldsymbol{p})\,, \end{aligned} \tag{5.8}$$

where we let $F = SJ^{-1}M$. Therefore, F is a $K \times L$ outage signature map determined by PMU locations, system operating states, and topology. Each column of F, i.e., F_l represents the incremental effect of line l outage on all bus voltage angles captured by PMUs.

Fig. 5.1 shows an example of F for a random placement of 19 PMUs on the New England 39-bus system, using J^{-1} obtained from steady-state bus voltages. The signature map captures the varying degree of impact each

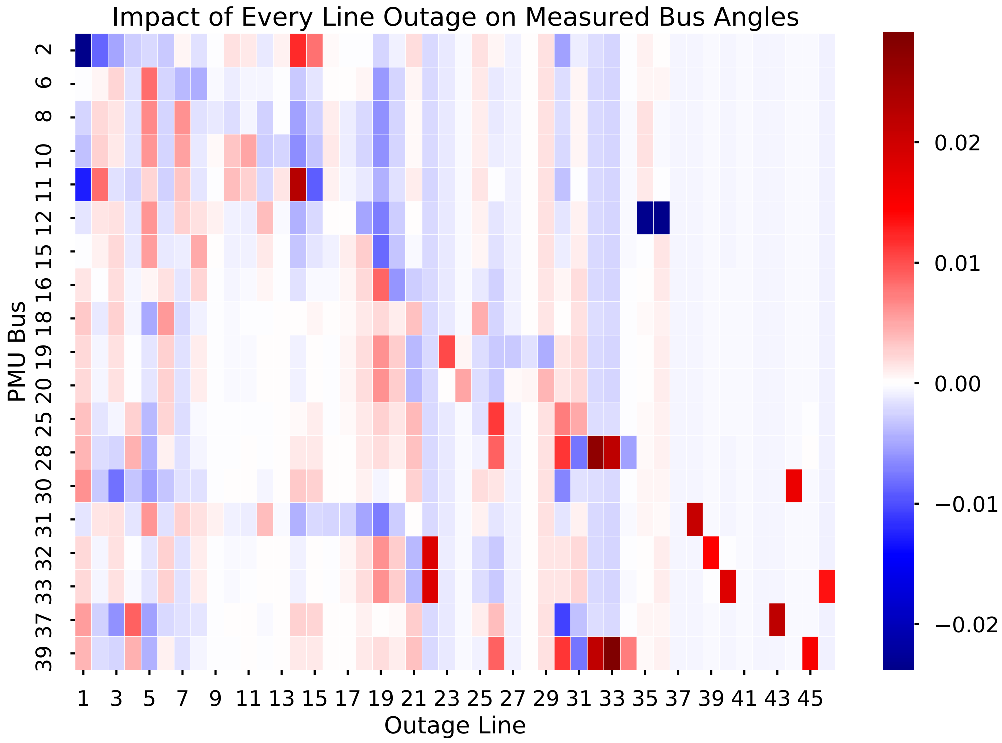

Figure 5.1: *An example of the* 19×46 *signature map constructed using a random placement of 19 PMUs in the New England 39-bus system with 46 transmission lines. Each column corresponds to a single line outage and its incremental impact on PMU-equipped bus voltage phase angles.*

line outage has on PMU-equipped buses. Outages of some lines might not be uniquely identified because they create similar phase angle responses, e.g., line 10 and 11, line 32 and 33. The map also suggests that some line outages create minimal impact that they might be indistinguishable from normal conditions, e.g., line 37 or line 41. While distinctive signatures from the map should be useful in identifying outage lines, we need to address the problem of indistinguishable line outages in order to fully exploit the signature map information.

5.3 Outage Identification Scheme

After a single- or multiple-line outage, the signature map developed in the previous section provide a basis for accurate outage identification. We assume that the outage event is detected quickly using a detection scheme, e.g., of [16] or [19]. We first formulate multiple-line outage identification as a sparse regression problem. Then, a method to address indistinguishable outages is proposed to further improve the regression result accuracy.

5.3.1 Identification by Sparse Regression

Suppose a simultaneous line outages happen at $l_i, i = 1, \ldots, a$ and the size is relatively small, i.e., $a \ll L$. Let $\boldsymbol{\beta}$ be an L-vector with all zeros except at $\boldsymbol{\beta}_{l_i}$ with value p_{l_i} for $i = 1, \ldots, a$. If the outage model in Section 5.2 holds, we can write

$$\begin{aligned}\Delta\boldsymbol{\theta} &= SJ^{-1}(m_{l_1}p_{l_1} + \cdots + m_{l_a}p_{l_a}) + \boldsymbol{\epsilon} \\ &= SJ^{-1}M\boldsymbol{\beta} + \boldsymbol{\epsilon} \\ &= F\boldsymbol{\beta} + \boldsymbol{\epsilon}\,, \end{aligned} \tag{5.9}$$

where M in the second step is as defined in (5.6) and $\boldsymbol{\epsilon}$ is a Gaussian noise term with mean zero and known variance $\sigma^2\mathbf{I}_{K\times K}$, representing measurement error of K PMUs. Hence, non-zero entries, or support, of the power transfer vector $\boldsymbol{\beta}$ reveal true outage locations. Given the signature map F and PMU measurements $\Delta\boldsymbol{\theta}$, $\boldsymbol{\beta}$ can be estimated from the above relationship by minimizing the squared-error loss, subject to the outage size constraint as

$$\min_{\boldsymbol{\beta}\in\mathbb{R}^L} \|\Delta\boldsymbol{\theta} - F\boldsymbol{\beta}\|_2^2\,, \tag{5.10}$$

$$\text{s.t. } \|\boldsymbol{\beta}\|_0 = a\,,$$

where $\|\cdot\|_2^2$ is the square of the ℓ_2 norm and $\|\cdot\|_0$ is the number of non-zero entries of a vector. However, as we do not known a priori the location of the non-zero entries, the above formulation presents a challenging combinatorial optimization problem. Methods such as exhaustive search, forward-stepwise regression or mix integer optimization could be used to solve the problem [74]. However, compared to shrinkage method, in particular lasso, they are computationally more intensive, thus not suitable for real-time application in realistic power systems [75].

Lasso was originally proposed in [76] and has since been used in various applications for ease of implementation, robustness to noise, and the ability to shrink some coefficients to exactly zero, thus recovering true support of the vector. Lasso solves a relaxed version of the problem in (5.10) by replacing the ℓ_0 constraint with an ℓ_1 constraint:

$$\min_{\boldsymbol{\beta}\in\mathbb{R}^L} \|\Delta\boldsymbol{\theta} - F\boldsymbol{\beta}\|_2^2 \,, \qquad \text{s.t. } \|\boldsymbol{\beta}\|_1 \leq a \,, \tag{5.11}$$

and equivalently in Lagrangian form:

$$\min_{\boldsymbol{\beta}\in\mathbb{R}^L} \left\{\|\Delta\boldsymbol{\theta} - F\boldsymbol{\beta}\|_2^2 + \lambda\|\boldsymbol{\beta}\|_1\right\} , \tag{5.12}$$

where $\|\cdot\|$ is the ℓ_1 norm and λ is a regularization parameter that has one-to-one correspondence to a for solutions of (5.11) and (5.12). Larger values of λ impose stronger regularization on $\boldsymbol{\beta}$, whereas if $\lambda = 0$, the lasso solution $\hat{\boldsymbol{\beta}}$ is the same as the least squares estimate. According to [77], given a fixed F, there exists a finite sequence,

$$\lambda_0 > \lambda_1 > \cdots > \lambda_Q = 0 \,, \tag{5.13}$$

such that 1) for all $\lambda > \lambda_0$, $\hat{\boldsymbol{\beta}} = \mathbf{0}$, 2) the support of $\hat{\boldsymbol{\beta}}$ does not change with λ for $\lambda_q < \lambda < \lambda_{q+1}$, $q = 0, \ldots, Q-1$. These λ_q's are called transition points as the support in lasso solution changes at each λ_q. Often, λ is selected according to some parameter tuning scheme, e.g. cross validation, such that the resultant regression model achieves best prediction accuracy. However, our objective is to uncover the true support of $\boldsymbol{\beta}$. Thus, lasso solution at various transition points need to be obtained each time an outage is detected to ascertain the location, and in effect the number, of outage lines.

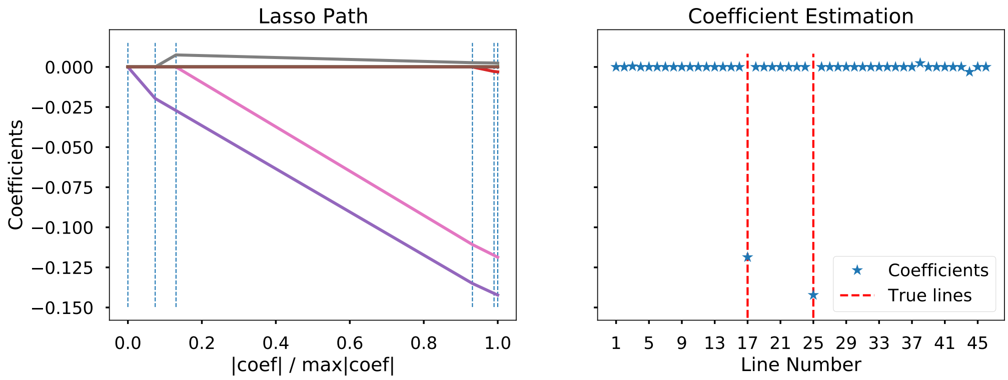

Figure 5.2: *Lasso path via LARS illustration for double-line outage at line 17 and 25. Complete lasso regularization path is shown on the left and coefficient estimation after five candidates entered the model on the right.*

Least angle regression (LARS), originally proposed by [78], with lasso modification is an efficient algorithm that computes the entire lasso path with a complexity of least squares regression. Briefly, starting with coefficients of zero, LARS identifies the first variable as the one most correlated with the response, e.g., $\Delta\boldsymbol{\theta}$. As the coefficients of the active variables move toward their least squares estimates, a new variable becomes active when its correlation with the residual "catches up" with the active set. These changes happen at the transitions points of (5.13) and variables enter one at a time [78]. The process is stopped after Q steps and in general $Q = \min\{K-1, L\}$ for standardized data unless otherwise specified.

Assuming $\Delta\boldsymbol{\theta}$, its mean $\Delta\bar{\boldsymbol{\theta}}$, signature map F, and the maximum number of non-zero entries Q are provided, LARS can produce a sequence of regularization parameters λ^q and the associated lasso solution $\boldsymbol{\beta}^q$ to (5.12) as described in Algorithm 2. Indices of siginificantly non-zero entries of $\boldsymbol{\beta}^Q$ are then identified as potential outage locations.

Fig. 5.2 shows an example of the lasso path computed using LARS for a double-line outage event. The final $\boldsymbol{\beta}$ has five non-zero coefficients after five transitions. The scheme correctly identifies line 17 and 25 as they have significantly non-zero estimated coefficients compared to the others.

Algorithm 2 Least Angle Regression with Lasso Modification

Input: $\Delta\boldsymbol{\theta}, \Delta\bar{\boldsymbol{\theta}}, F, Q$

Output: Lasso solution path $\{\lambda_q, \boldsymbol{\beta}^q\}_{q=0}^{Q}$

1: Standardize columns of F to mean zero and unit ℓ_2 norm. Set $\boldsymbol{\beta}^0 = (\beta_1, \beta_2, \ldots, \beta_L) = \mathbf{0}$. Let $r_0 = \Delta\boldsymbol{\theta} - \Delta\bar{\boldsymbol{\theta}}$.

2: Get first active column:

$$j = \arg\max_{i \in \mathcal{L}} |\langle r_0, F_i \rangle| \,.$$

Let $\lambda_0 = |\langle r_0, F_j \rangle|$. Define $\mathcal{A} = \{j\}$ and $F_{\mathcal{A}}$ as the active set and signature matrix with columns from the set.

3: **for** $q = 1, 2, \ldots, Q$ **do**

4: Get current least-squares direction: $\delta = \frac{1}{\lambda_{q-1}}(F_{\mathcal{A}}^\top F_{\mathcal{A}})^{-1} F_{\mathcal{A}}^\top r_{q-1}$. Define L-vector $\mathbf{u}$ such that $\mathbf{u}_{\mathcal{A}} = \delta$ and zero everywhere else.

5: Move coefficients toward least-squares estimate: $\boldsymbol{\beta}(\lambda) = \boldsymbol{\beta}^{q-1} + (\lambda_{q-1} - \lambda)\mathbf{u}$, for $0 < \lambda \leq \lambda_{q-1}$ while maintaining $r(\lambda) = \Delta\boldsymbol{\theta} - F\boldsymbol{\beta}(\lambda)$. Drop any element of $\mathcal{A}$ if the corresponding coefficient crosses 0 and recompute the least-squares estimate.

6: Identify the largest λ at which $|\langle r(\lambda), F_l \rangle| = \lambda$ for $l \notin \mathcal{A}$. Let $\lambda_p = \lambda$, the new transition point.

7: Suppose the new active column has index j. Update $\mathcal{A} = \mathcal{A} \cup j$, $\boldsymbol{\beta}^q = \boldsymbol{\beta}(\lambda_q) + (\lambda_{q-1} - \lambda_q)\mathbf{u}$, and $r_q = \Delta\boldsymbol{\theta} - F\boldsymbol{\beta}^q$.

8: **end for**

9: Return the sequence $\{\lambda_q, \boldsymbol{\beta}^q\}_0^Q$.

The third-highest coefficient corresponds to line 38 which is a neighbor of line 17 that likely produces similar outage response. It enters the model before line 17 does. However its coefficient is overtaken by that of line 17 as they increase towards the least squares solution, giving the correct final identification result.

5.3.2 Indistinguishable Line Outages

As seen from the signature map of Fig. 5.1, some outages create highly similar responses from the system, i.e., $F_i \approx F_j$ for some $i, j \in \mathcal{L}$. In general, this ambiguity problem is commonly encountered in realistic systems [17]. One reason is that some line outages do indeed create similar responses due to a combination of topological positions and pre-outage power flow carried.

On the other hand, a limited PMU deployment might mean distinctive signatures of some outages are not observable. Intuitively, the second situation is more pronounced as the PMU budget decreases. It is also well-known that with a group of highly correlated predictors, the lasso formulation of (5.12) tends to select one from the group and does not care which one to select [79]. In the extreme case where $F_i = F_j$ for some $i, j \in \mathcal{L}$ and $\hat{\boldsymbol{\beta}}$ is the lasso solution, it can be shown that $\hat{\beta}_i \hat{\beta}_j \geq 0$ and $\hat{\boldsymbol{\beta}}^*$ is another solution of (5.12) where

$$\hat{\beta}^*_k = \begin{cases} \hat{\beta}_k \,, k \neq i, k \neq j \\ (\hat{\beta}^*_i + \hat{\beta}^*_j)s \,, k = i \\ (\hat{\beta}^*_i + \hat{\beta}^*_j)(1-s) \,, k = j \,, \end{cases} \tag{5.14}$$

for some $s \in [0, 1]$ and $k \in \mathcal{L}$. Therefore, lasso might not have a unique solution when predictors are highly correlated.

In the context of our identification problem, the true outage line, e.g., i, might not be correctly identified if $F_i \approx F_j$, and equivalently their correlation is close to 1,

$$\mathrm{corr}(p_i F_i, p_j F_j) = \mathrm{corr}(F_i, F_j) \approx 1 \,,$$

for some $i, j \in \mathcal{L}$. To address this ambiguity problem, we propose to group transmission lines into minimal diagnosable clusters (MDCs). Each MDC contains lines which, given a fixed PMU placement, produce responses that our lasso formulation could not distinguish with a high probability. Concretely, we define MDC as a group of lines whose observable outage effects have pairwise correlations higher than a pre-defined threshold ρ^*. Therefore, the MDC of line i is

$$g_i = \{j : \mathrm{corr}(F_i, F_j) \geq \rho^*\} \,, \tag{5.15}$$

for $j \in \mathcal{L} \setminus i$. The collection of MDCs for all transmission lines is

$$G_F = \{g_1, g_2, \ldots, g_L\} \,. \tag{5.16}$$

Also, the diagnosability of a system with given PMU locations can be characterized by the proportion of single-element MDCs,

$$V(\rho^*) = \left(\sum_{i=1}^{L} \mathbf{1}(|g_i| = 1) \right) / L \, ,$$

where $\mathbf{1}(\cdot)$ is indicator function and $|g|$ counts the number of elements in the set g.

Intuitively, a smaller ρ^* corresponds to a more relaxed correlation requirement to enter the MDC, therefore in general decreases $V(\rho^*)$ and vice versa. With MDCs constructed offline, they can augment the lasso solution in real-time outage identification. Suppose $L_o = \{l_i^*, i = 1, \ldots, a\}$ are identified by lasso as outage lines. The augmented solution set would be

$$L_o^* = \{g_{l_1^*} \cup \cdots \cup g_{l_a^*}\} \, . \tag{5.17}$$

With MDC augmentation, outage identification accuracy is improved, however, potentially at the expense of identification precision. The trade-off is controlled through the correlation threshold. The effect of the threshold and accuracy-precision trade-off is investigated further in simulation study of Section 5.4.

To end this section, we summarize the proposed identification scheme in Fig. 5.3. The scheme is split into an offline and online part. Preparation work of step one to three could be done offline since they only require quasi-steady state information and baseline system parameters. Once the signature map and MDCs are constructed, they could be used in real-time monitoring operation as in step four to six.

The idea of constructing expected angle change based on power injection to identify outage lines is not new [17, 18, 27]. Separately, authors in [43] and [45] have also formulated outage identification as a sparse vector recovery problem. However our work is different in the following aspects: 1) All except [18] have relied on the simplified DC power flow model by assuming a flat voltage profile and approximately identical phase angles. Our signature map is derived from the AC power flow model, better reflecting the

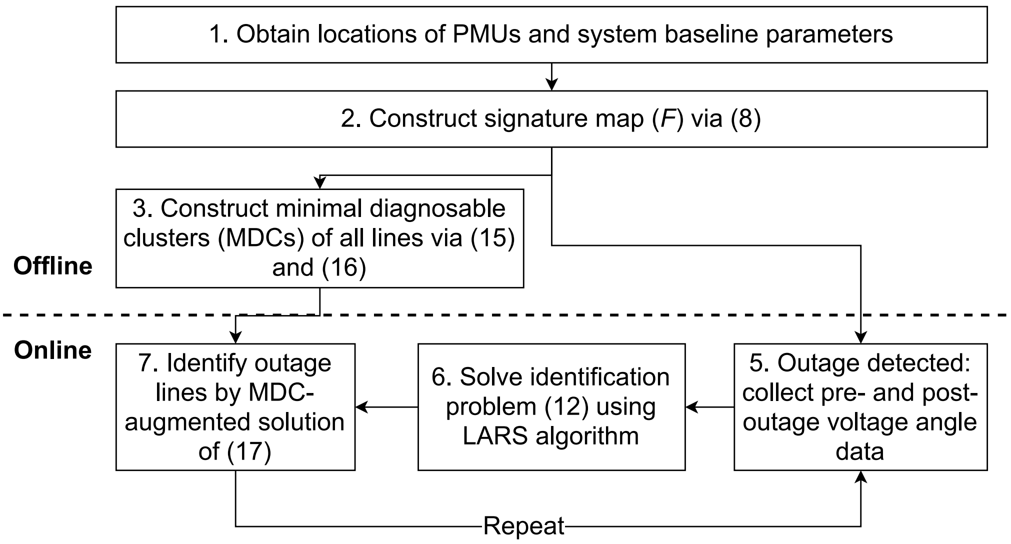

Figure 5.3: *Framework of the proposed line outage identification scheme. Preparation steps one to three can be performed offline while outage identification steps four to six can be carried out during real-time monitoring operations.*

heterogeneous operating condition of power systems. 2) All except [17] do not consider the impact of indistinguishable outage events on identification performance. Whereas Wu *et al.*conduct online search for indistinguishable outage locations, our MDCs are constructed in advance and incur no extra computation during real-time identification. 3) Enriquez *et al.*uses both voltage and current phasor for identification while our method only requires voltage measurements [18]. Performance of a sparse regression-based [43] and an AC power flow-based method [18] are compared in our simulation study.

5.4 Simulation Study

5.4.1 Simulation Setting

We test our identification scheme on IEEE 39-bus New England test system [53]. System transient responses following an outage are simulated using the open-source simulation package COSMIC [54] in which a third-order machine model and AC power flow model are used. We assume that the sampling frequency of a PMU is 30 samples per second. The system loads are varied by a random percentage between -5% and 5% from the base-line values for each simulation run. The total duration of a run is 10 seconds; the outage takes place at the 3rd second. Pre- and post-outage voltage phase angles are obtained at the 1st and 10th second. Artificial noise is added to all sampled angle data, $\Delta\boldsymbol{\theta}$, to account for system and measurement noise. They are drawn from a Gaussian distribution with mean $\mathbf{0}$ and standard deviation fo 5% of the pre-outage $\Delta\boldsymbol{\theta}$ on respective buses.

Simulated single-line outages include line 1 to 36 except line 21 as it creates two islands. Double-line outages include 100 random pairs of lines from line 1 to 46 that does not create separate islands. Given a list of identified and true outage lines, L_o and L_{true}, identification performance is assessed by Accuracy (A),

$$A(L_o, L_{true}, a) := \frac{\sum_i \mathbf{1}(|L_{o,i} \cap L_{true,i}| = a)}{|L_{true}|}, \tag{5.18}$$

Therefore, the accuracy of single-line outage identification of a scheme is $A(L_o, L_{true}, 1)$. Similarly, the "half-correct" and "all-correct" accuracy of double-line outage is $A(L_o, L_{true}, 1)$ and $A(L_o, L_{true}, 2)$. Accuracy with MDC augmentation for each scenario is obtained by replaceing L_o with L_o^*, the augmented set defined in (5.17).

5.4.2 Illustrative Outage Identification Example

Using the same example of a double-line outage at line 17 and 25, Fig. 5.4 demonstrates limited observability (top) and the estimation of $\Delta\boldsymbol{\theta}$ by each method (bottom). The angle change estimation is obtained using recovered power transfer coefficient $\hat{\boldsymbol{\beta}}$, i.e., $\Delta\hat{\boldsymbol{\theta}} = F\hat{\boldsymbol{\beta}}$. Limited deployment of PMUs means some bus angles are not observed. This is illustrated in the top figure where some signatures of the outage are not missed. If unobserved locations contain all the distinctive signatures of that outage, distinguishing it from the others would be challenging. Therefore, characterizing and exploiting line diagnosabilities through MDCs are necessary to overcome this challenge.

The bottom figure shows a comparison of $\Delta\hat{\boldsymbol{\theta}}$ by three methods under comparison. Columns of F corresponding to the outage lines identified by each method are used. AC power flow-based methods are clearly better at reconstructing the angle changes than the DC one. Notice that the DC estimation has more "flat" angles than the other two, thus fewer details to distinguish it from other outages. While variable selection accuracy rather than estimation accuracy is our focus, this figure nevertheless demonstrates the superior performance of AC power flow model at capturing a more nuanced outage impact.

5.4.3 Average Identification Performance

Average performance of each identification scheme is reported based on 200 simulation runs over all the single- and double-line outages. Random noises and PMU placements of a 25% or 50% PMU coverage are used in each run. Two existing methods are compared, namely "DC" for the DC power flow-based method in [43] and "Corr" for the AC power flow-based method in [18]. Performance gain with MDC augmentation of (5.17) is also reported under the name "...+MDC".

5.4.3.1 Single-line outage

Fig. 5.5 shows the identification results for single-line outage. With or without MDC augmentation, correlation-based method and the proposed method consistently outperform the DC-based method in both cases of PMU coverage. The former two methods are roughly always 40% more accurate than the DC-based method. Correlation-based method achieves almost identical result with the proposed method regardless of MDC augmentation or PMU coverage. This is expected since the proposed method identifies the first variable as the one most correlated with the response, an identifical procedure as the correlation-based method.

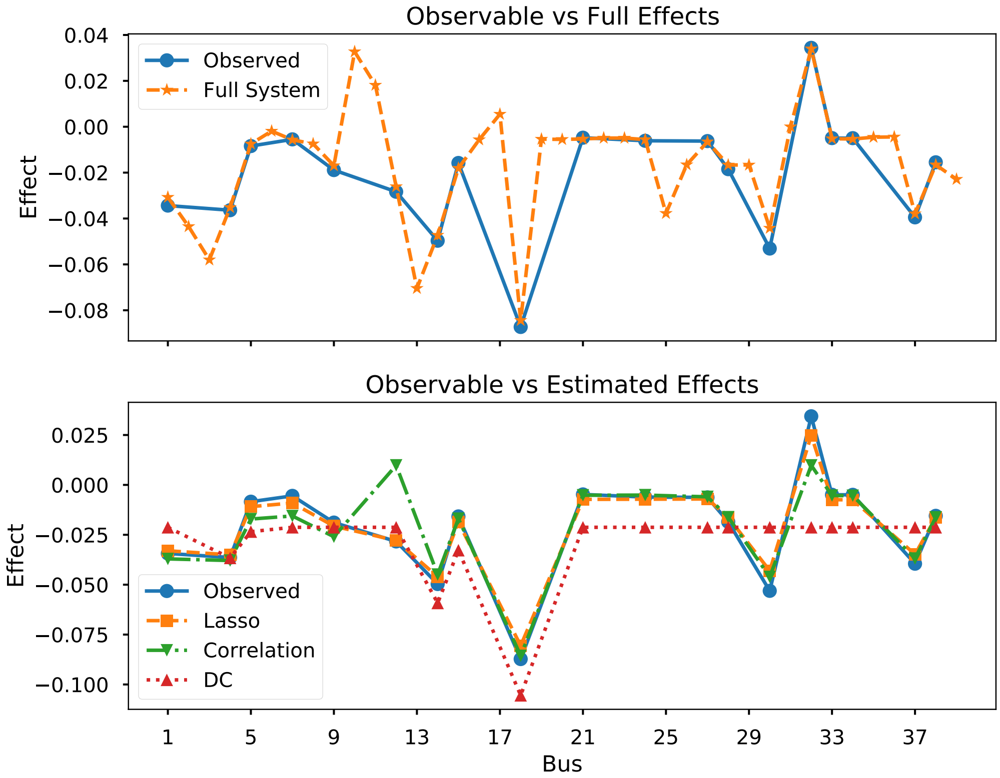

Figure 5.4: *Full, observed, and estimated outage impact on bus voltage phase angles after a double-line outage at line 17 and 25. 19 out of 39 buses are equipped with PMUs. The top figure shows observed noisy data with true and complete system states. The bottom figure compares the estimated phase angles changes from three methods against the observed states.*

When PMU coverage is increased from 25% to 50%, improvements in identification accuracy across all methods are observed as expected. Under a 25% coverage, the proposed method is 52% and 86% accurate (median), without and with MDC augmentation. With a 50% coverage, the performance is 72% and 93%. Lastly, augmenting original solution with their MDCs improves accuracy across methods and PMU coverages. Roughly speaking, MDC augmentation improves accuracy by 30% for the 25% coverage and 20% for the 50% coverage. Notably, the two AC-based methods reach 93% identification accuracy under a 50% coverage with MDCs. The decrease in accuracy improvement for better observed system

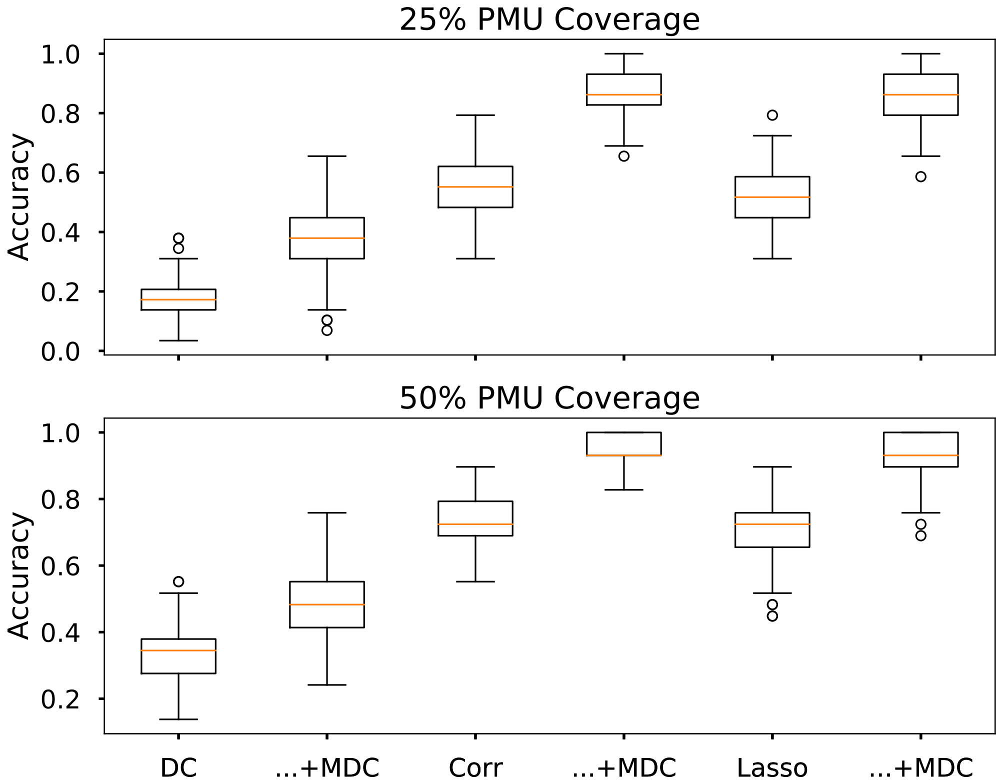

Figure 5.5: *Box-plots of single-line outage identification results for DC-based, correlation-based, and the proposed method. Results are based on 200 random simulation runs under a 25% (top) and 50% (bottom) PMU coverage in the New England 39-bus system. Each method has two sets of results: accuracy of the original identification and of that augmented with MDCs.*

might be bacause they tend to have more distinguishable outages.

5.4.3.2 Double-line outage

Fig. 5.6 shows the identification results for double-line outage. The proposed method consistently outperforms the other two methods, especially in the “all correct" case. DC-based method performs worst in both categories. The correlation-based method is not as accurate beyond the identification of the first line. The reason might be that the proposed formulation treats $\boldsymbol{p}'$ as an unknown vector. It is systematically estimated from data by lasso. However the correlation-based method treats it as a

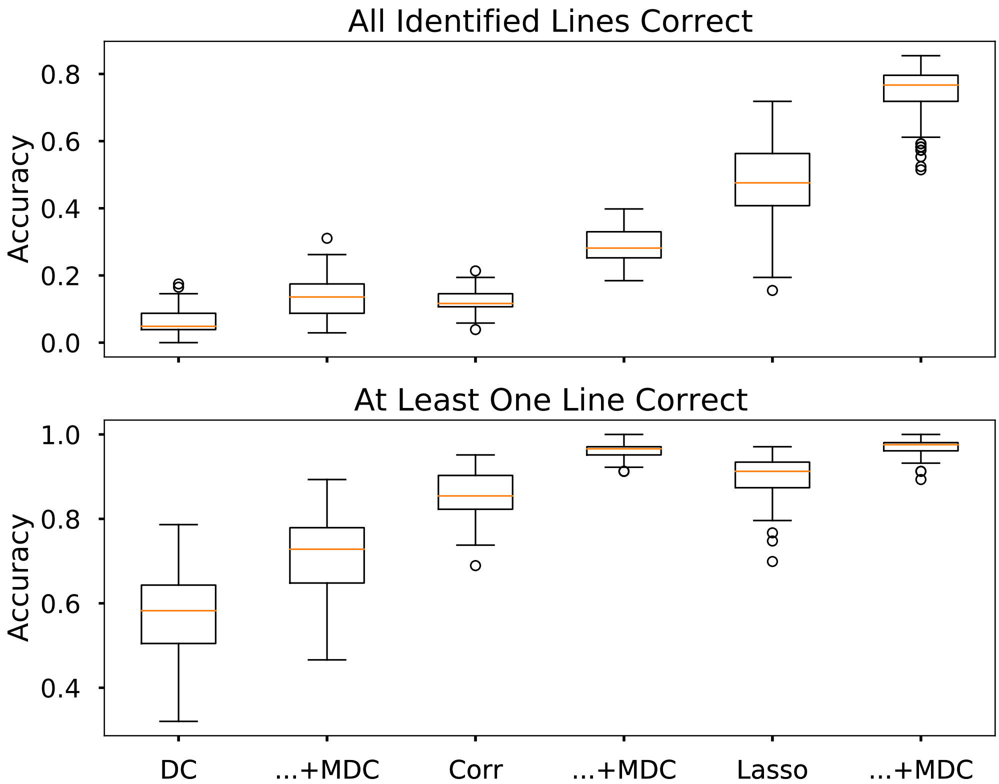

Figure 5.6: *Box-plots of double-line outage identification results for DC-based, correlation-based, and the proposed method. "All correct" (top) and "half correct" (bottom) results are based on 200 random simulation runs under a 50% PMU coverage in the New England 39-bus system. Each method has two sets of results: accuracy of the original identification and of that augmented with MDCs.*

fixed vector of line reactance. Inaccuracy in the model might then lead to inaccurate identification of multiple outage lines. Again, augmenting solutions with MDCs improve accuracy for all methods, especially in the "all correct" category. Overall, the proposed method with MDC augmentation (Lasso+MDC) achieves the best performance. It can identify 80% of the simulated double-line outages under a 50% PMU coverage.

5.4.3.3 Effect of minimal diagnosable cluster

Table 5.1 shows the trade-off between identification precision and accuracy by varying the MDC threshold ρ^* in (5.15). As expected, the proportion

Table 5.1: Impact of Minimal Diagnosable Cluster Threshold on Identification Precision-Accuracy Trade-off Using Lasso+MDC

Threshold (ρ^*)	Single-element MDC (%)	Single-line	Double-line
0.80	0.34 (0.06)	0.94 (0.06)	0.69 (0.08)
0.84	0.42 (0.06)	0.94 (0.05)	0.69 (0.07)
0.88	0.49 (0.07)	0.95 (0.05)	0.69 (0.08)
0.93	0.55 (0.06)	0.93 (0.06)	0.67 (0.09)
0.95	0.58 (0.06)	0.93 (0.07)	0.66 (0.09)
0.98	0.62 (0.06)	0.92 (0.06)	0.66 (0.09)
0.99	0.68 (0.07)	0.89 (0.07)	0.61 (0.09)

of single-element MDC, $V(\rho^*)$, increases as the threshold approaches 1. In particular, a threshold of $\rho^* = 0.8$ leads to 34% MDCs with a single element. That proportion increases to 68% when $\rho^* = 0.99$. The good news is, a tighter requirement on MDC does not lead to much decrease in single- and double-line outage identification accuracy using the proposed method, from 94% to 89% and 69% to 61%, respectively.

Therefore, augmenting solution with MDCs could substantially improve identification accuracy while sacrificing a moderate amount of identification precision. The result also suggests that recognizing the most highly correlated line outages, e.g., setting $\rho^* \geq 0.95$, is enough to reap the benefit of MDC augmentation. Nevertheless, there is a trade-off between accuracy and precision. The threshold could be determined in conjunction with decision-makers' other considerations, e.g., resources available or criticality of the system.

5.4.3.4 Effect of measurement noise

We also report the performance of the proposed method with respect to measurement noise in Fig. 5.7. The performance is largely robust to measurement noise. The accuracy for single-line identification shows no clear difference as the noise level increases. There is a moderate decrease in accuracy for double-line outage identification as the noise level increases to 10%. Lasso formulation is known to be robust to noise [75]. This is corroborated by results from our simulation study.

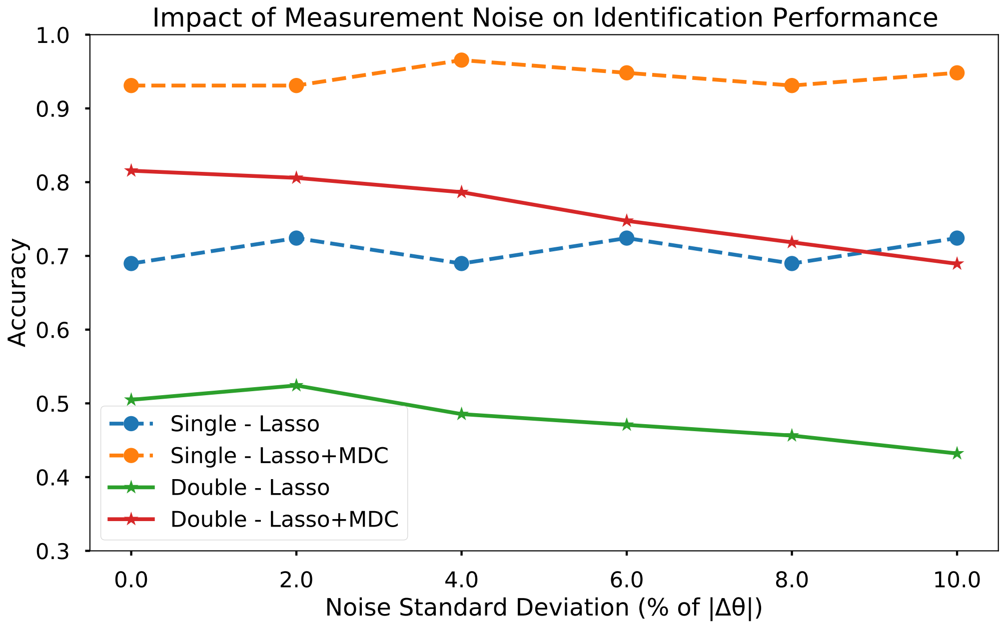

Figure 5.7: *Impact of measurement noise on identification performance of the proposed method. Performance using data with noise standard deviation varying from 0% to 10% of* $|\Delta\boldsymbol{\theta}|$ *is reported by median accuracy of single- and double-line outages using Lasso and Lasso+MDC.*

5.5 Conclusion

In this paper, we propose a novel framework of real-time multiple-line outage identification with limited PMU deployment. AC power flow model is utilized to construct a signature map that encodes voltage phase angle signatures of each line outage. Identification is then formulated into an underdetermined sparse regression problem solved by lasso. Minimal diagnosable clusters are proposed to further improve identification accuracy. Single-line and double-line outages simulated on the New England 39-bus system with 25% and 50% PMU deployment are used to study the proposed method's performance. The proposed method is shown to have better identification accuracy under all simulation settings, especially for double-line outages. The robustness of the method is also demonstrated using varying levels of noisy data. Finally, we have also shown the merit of exploiting line diagnosability through minimal diagnosable cluster which significantly improves identification accuracy by trading off a small amount of precision.

We did not however consider the problem of post-outage system parameter recovery in this work. In general, online updating of system parameters under a partial observability remains a challenging and important task that is worth investigating. Also, the diagnosability of line outage is intimately related to where the limited number of PMUs are placed. We intend to study the optimal PMU placement problem for line outage identification in our future research.

Chapter 6

Conclusion

Bibliography

[1] J. Ellis, D. Fisher, T. Longstaff, L. Pesante, and R. Pethia, "Report to the president's commission on critical infrastructure protection." Carnegie-Mellon Univ Pittsburgh PA Software Engineering Inst, Tech. Rep., 1997.

[2] S. D. Guikema, "Natural disaster risk analysis for critical infrastructure systems: An approach based on statistical learning theory", *Reliability Engineering & System Safety*, vol. 94, no. 4, pp. 855–860, 2009.

[3] M. Amin, "Challenges in reliability, security, efficiency, and resilience of energy infrastructure: Toward smart self-healing electric power grid", in *2008 IEEE Power and energy society general meeting-conversion and delivery of electrical energy in the 21st century*, IEEE, 2008, pp. 1–5.

[4] J. Seymour and T. Horsley, "The seven types of power problems", *APC, USA*, 2005.

[5] M. Kezunovic, L. Xie, and S. Grijalva, "The role of big data in improving power system operation and protection", in *2013 IREP Symposium Bulk Power System Dynamics and Control-IX Optimization, Security and Control of the Emerging Power Grid*, IEEE, 2013, pp. 1–9.

[6] F. Aminifar, M. Fotuhi-Firuzabad, A. Safdarian, A. Davoudi, and M. Shahidehpour, "Synchrophasor measurement technology in power systems: panorama and state-of-the-art", *IEEE Access*, vol. 2, pp. 1607–1628, 2014.

[7] FERC and NAERC, "Arizona-Southern California outages on September 8, 2011: Causes and recommendations", Tech. Rep., 2012.

[8] F. Milano, “Power System Modelling and Scripting”, Springer Science & Business Media, 2010.

[9] M. Pignati, M. Popovic, S. Barreto, R. Cherkaoui, G. D. Flores, J.-Y. Le Boudec, M. Mohiuddin, M. Paolone, P. Romano, S. Sarri, *et al.*, “Real-time state estimation of the epfl-campus medium-voltage grid by using pmus”, in *2015 IEEE Power & Energy Society Innovative Smart Grid Technologies Conference*, IEEE, 2015, pp. 1–5.

[10] M. Abdi-Khorsand and V. Vittal, “Modeling protection systems in time-domain simulations: a new method to detect mis-operating relays for unstable power swings”, *IEEE Transactions on Power Systems*, vol. 32, no. 4, pp. 2790–2798, 2017.

[11] E. Mohamed, W. Elballa, A. Karrar, G. Kobet, and A. Eltom, “Fast line outage detection using pmu measurements in partially observed networks”, in *2018 IEEE Power & Energy Society General Meeting*, IEEE, 2018, pp. 1–5.

[12] T. Kim and S. J. Wright, “PMU placement for line outage identification via multinomial logistic regression”, *IEEE Transactions on Smart Grid*, vol. 9, no. 1, pp. 122–131, 2018.

[13] A. Chakrabortty, J. H. Chow, and A. Salazar, “Interarea model estimation for radial power system transfer paths with intermediate voltage control using synchronized phasor measurements”, *IEEE Transactions on Power Systems*, vol. 24, no. 3, pp. 1318–1326, 2009.

[14] G. Chavan, M. Weiss, A. Chakrabortty, S. Bhattacharya, A. Salazar, and F. H. Ashrafi, “Identification and predictive analysis of a multi-area wecc power system model using synchrophasors”, *IEEE Transactions on Smart Grid*, vol. 8, no. 4, pp. 1977–1986, 2017.

[15] F. Aminifar, M. Fotuhi-Firuzabad, A. Safdarian, A. Davoudi, and M. Shahidehpour, “Synchrophasor measurement technology in power systems: Panorama and state-of-the-art”, *IEEE Access*, vol. 2, pp. 1607–1628, 2014.

[16] X. Yang, N. Chen, and C. Zhai, “A control chart approach to power system line outage detection under transient dynamics”, *IEEE Transactions on Power Systems*, vol. 36, no. 1, pp. 127–135, 2021.

[17] J. Wu, J. Xiong, and Y. Shi, “Efficient location identification of multiple line outages with limited pmus in smart grids”, *IEEE Transactions on Power Systems*, vol. 30, no. 4, pp. 1659–1668, 2015.

[18] N. Costilla-Enríquez, C. R. Fuerte-Esquivel, and V. J. Gutiérrez-Martínez, “A sensitivity-based approach for the detection of multiple-line outages using phasor measurements”, *IEEE Transactions on Power Systems*, vol. 34, no. 5, pp. 3697–3705, 2019.

[19] X. Yang, N. Chen, and C. Zhai, “A particle filter approach to power system line outage detection using load and generator bus dynamics”, 2021. arXiv: 2107.06754 `[eess.SY]`.

[20] L. Xie, Y. Chen, and P. R. Kumar, “Dimensionality reduction of synchrophasor data for early event detection: Linearized analysis”, *IEEE Transactions on Power Systems*, vol. 29, no. 6, pp. 2784–2794, 2014.

[21] M. Rafferty, X. Liu, D. M. Laverty, and S. McLoone, “Real-time multiple event detection and classification using moving window PCA”, *IEEE Transactions on Smart Grid*, vol. 7, no. 5, pp. 2537–2548, 2016.

[22] S. Hosur and D. Duan, “Subspace-driven output-only based change-point detection in power systems”, *IEEE Transactions on Power Systems*, vol. 34, no. 2, pp. 1068–1076, 2019.

[23] M. Jamei, A. Scaglione, C. Roberts, E. Stewart, S. Peisert, C. McParland, and A. McEachern, “Automated anomaly detection in distribution grids using upmu measurements”, in *Proceedings of the 50th Hawaii International Conference on System Sciences*, 2017, pp. 3184–3193.

[24] ——, “Anomaly detection using optimally placed μPMU sensors in distribution grids”, *IEEE Transactions on Power Systems*, vol. 33, no. 4, pp. 3611–3623, 2017.

[25] O. Ardakanian, Y. Yuan, R. Dobbe, A. von Meier, S. Low, and C. Tomlin, “Event detection and localization in distribution grids with phasor measurement units”, in *2017 IEEE Power & Energy Society General Meeting*, IEEE, 2017, pp. 1–5.

[26] O. Ardakanian, V. W. Wong, R. Dobbe, S. H. Low, A. von Meier, C. J. Tomlin, and Y. Yuan, “On identification of distribution grids”, *IEEE Transactions on Control of Network Systems*, vol. 6, no. 3, pp. 950–960, 2019.

[27] J. E. Tate and T. J. Overbye, “Line outage detection using phasor angle measurements”, *IEEE Transactions on Power Systems*, vol. 23, no. 4, pp. 1644–1652, 2008.

[28] J. E. Tate and T. J. Overbye, “Double line outage detection using phasor angle measurements”, in *2009 IEEE Power & Energy Society General Meeting*, IEEE, 2009, pp. 1–5.

[29] Z. Dai and J. E. Tate, “Line outage identification based on ac power flow and synchronized measurements”, in *2020 IEEE Power & Energy Society General Meeting (PESGM)*, IEEE, 2020, pp. 1–5.

[30] Y. C. Chen, T. Banerjee, A. D. Dominguez-Garcia, and V. V. Veeravalli, “Quickest line outage detection and identification”, *IEEE Transactions on Power Systems*, vol. 31, no. 1, pp. 749–758, 2016.

[31] G. Rovatsos, X. Jiang, A. D. Dominguez-Garcia, and V. V. Veeravalli, “Statistical power system line outage detection under transient dynamics”, *IEEE Transactions on Signal Processing*, vol. 65, no. 11, pp. 2787–2797, 2017.

[32] M. Babakmehr, M. G. Simões, M. B. Wakin, and F. Harirchi, “Compressive sensing-based topology identification for smart grids”, *IEEE*

Transactions on Industrial Informatics, vol. 12, no. 2, pp. 532–543, 2016.

[33] M. Babakmehr, M. G. Simoes, A. Al-Durra, F. Harirchi, and Q. Han, "Application of compressive sensing for distributed and structured power line outage detection in smart grids", in *2015 American Control Conference (ACC)*, IEEE, 2015, pp. 3682–3689.

[34] J. D. Glover, M. S. Sarma, and T. Overbye, "Power System Analysis & Design, SI Version", Cengage Learning, 2012.

[35] Q. Huang, L. Shao, and N. Li, "Dynamic detection of transmission line outages using Hidden Markov Models", *IEEE Transactions on Power Systems*, vol. 31, no. 3, pp. 2026–2033, 2016.

[36] W. Pan, Y. Yuan, H. Sandberg, J. Gonçalves, and G. B. Stan, "Online fault diagnosis for nonlinear power systems", *Automatica*, vol. 55, pp. 27–36, 2015.

[37] C. Yang, Z. H. Guan, Z. W. Liu, J. Chen, M. Chi, and G. L. Zheng, "Wide-area multiple line-outages detection in power complex networks", *International Journal of Electrical Power and Energy Systems*, vol. 79, pp. 132–141, 2016.

[38] J. Yu, Y. Weng, and R. Rajagopal, "PaToPa: A data-driven parameter and topology joint estimation framework in distribution grids", *IEEE Transactions on Power Systems*, vol. 33, no. 4, pp. 4335–4347, 2018.

[39] ——, "PaToPaEM: A data-driven parameter and topology joint estimation framework for time-varying system in distribution grids", *IEEE Transactions on Power Systems*, vol. 34, no. 3, pp. 1682–1692, 2019.

[40] M. Garcia, T. Catanach, S. Vander Wiel, R. Bent, and E. Lawrence, "Line outage localization using phasor measurement data in transient state", *IEEE Transactions on Power Systems*, vol. 31, no. 4, pp. 3019–3027, 2016.

[41] W. Li, D. Deka, M. Chertkov, and M. Wang, “Real-time faulted line localization and pmu placement in power systems through convolutional neural networks”, *IEEE Transactions on Power Systems*, vol. 34, no. 6, pp. 4640–4651, 2019.

[42] Y. Zhao, J. Chen, and H. V. Poor, “A learning-to-infer method for real-time power grid multi-line outage identification”, *IEEE Transactions on Smart Grid*, vol. 11, no. 1, pp. 555–564, 2020.

[43] H. Zhu and G. B. Giannakis, “Sparse overcomplete representations for efficient identification of power line outages”, *IEEE Transactions on Power Systems*, vol. 27, no. 4, pp. 2215–2224, 2012.

[44] R. Emami and A. Abur, “External system line outage identification using phasor measurement units”, *IEEE Transactions on Power Systems*, vol. 28, no. 2, pp. 1035–1040, 2013.

[45] J. C. Chen, W. T. Li, C. K. Wen, J. H. Teng, and P. Ting, “Efficient identification method for power line outages in the smart power grid”, *IEEE Transactions on Power Systems*, vol. 29, no. 4, pp. 1788–1800, 2014.

[46] P. Murty, “Power Systems Analysis”, Butterworth-Heinemann, 2017.

[47] P. Anderson and A. Bose, “Stability simulation of wind turbine systems”, *IEEE Transactions on Power Apparatus and Systems*, no. 12, pp. 3791–3795, 1983.

[48] R. Kaye and F. Wu, “Analysis of linearized decoupled power flow approximations for steady-state security assessment”, *IEEE Transactions on Circuits and Systems*, vol. 31, no. 7, pp. 623–636, 1984.

[49] D. R. Cox, “The Theory of Stochastic Processes”, Routledge, 2017.

[50] G. Lorden *et al.*, “Procedures for reacting to a change in distribution”, *The Annals of Mathematical Statistics*, vol. 42, no. 6, pp. 1897–1908, 1971.

[51] T. L. Lai, “Information bounds and quick detection of parameter changes in stochastic systems”, *IEEE Transactions on Information Theory*, vol. 44, no. 7, pp. 2917–2929, 1998.

[52] Y. Mei, “Efficient scalable schemes for monitoring a large number of data streams”, *Biometrika*, vol. 97, no. 2, pp. 419–433, 2010.

[53] T. Athay, R. Podmore, and S. Virmani, “A practical method for the direct analysis of transient stability”, *IEEE Transactions on Power Apparatus and Systems*, no. 2, pp. 573–584, 1979.

[54] J. Song, E. Cotilla-Sanchez, G. Ghanavati, and P. D. H. Hines, “Dynamic modeling of cascading failure in power systems”, *IEEE Transactions on Power Systems*, vol. 31, no. 3, pp. 2085–2095, 2016.

[55] M. Brown, M. Biswal, S. Brahma, S. J. Ranade, and H. Cao, “Characterizing and quantifying noise in PMU data”, in *IEEE Power and Energy Society General Meeting*, 2016, pp. 1–5.

[56] D. C. Montgomery, “Introduction to Statistical Quality Control”, John Wiley & Sons, 2007.

[57] P. Kundur, N. J. Balu, and M. G. Lauby, “Power system stability and control”, McGraw-Hill New York, 1994.

[58] P. W. Sauer, M. A. Pai, and J. H. Chow, “Power system dynamics and stability: with synchrophasor measurement and power system toolbox”, John Wiley & Sons, 2017.

[59] C. A. Lowry, W. H. Woodall, C. W. Champ, and S. E. Rigdon, “A multivariate exponentially weighted moving average control chart”, *Technometrics*, vol. 34, no. 1, pp. 46–53, 1992.

[60] S. E. Rigdon, “An integral equation for the in-control average run length of a multivariate exponentially weighted moving average control chart”, *Journal of Statistical computation and simulation*, vol. 52, no. 4, pp. 351–365, 1995.

[61] S. Knoth, “Arl numerics for mewma charts”, *Journal of Quality Technology*, vol. 49, no. 1, pp. 78–89, 2017.

[62] J. Zhao, M. Netto, and L. Mili, “A robust iterated extended kalman filter for power system dynamic state estimation”, *IEEE Transactions on Power Systems*, vol. 32, no. 4, pp. 3205–3216, 2017.

[63] S. Wang, W. Gao, and A. P. Meliopoulos, “An alternative method for power system dynamic state estimation based on unscented transform”, *IEEE Transactions on Power Systems*, vol. 27, no. 2, pp. 942–950, 2012.

[64] Y. Cui and R. Kavasseri, “A particle filter for dynamic state estimation in multi-machine systems with detailed models”, *IEEE Transactions on Power Systems*, vol. 30, no. 6, pp. 3377–3385, 2015.

[65] V. Kadirkamanathan, P. Li, M. H. Jaward, and S. G. Fabri, “Particle filtering-based fault detection in non-linear stochastic systems”, *International Journal of Systems Science*, vol. 33, no. 4, pp. 259–265, 2002.

[66] O. Cappé, S. J. Godsill, and E. Moulines, “An overview of existing methods and recent advances in sequential monte carlo”, *Proceedings of the IEEE*, vol. 95, no. 5, pp. 899–924, 2007.

[67] N. J. Gordon, D. J. Salmond, and A. F. Smith, “Novel approach to nonlinear/non-gaussian Bayesian state estimation”, *IEE Proceedings, Part F: Radar and Signal Processing*, vol. 140, no. 2, pp. 107–113, 1993.

[68] A. Doucet and A. M. Johansen, “A tutorial on particle filtering and smoothing: Fifteen years later”, *Handbook of nonlinear filtering*, vol. 12, no. 656-704, p. 3, 2009.

[69] J. S. Liu, “Monte Carlo strategies in scientific computing”, Springer Science & Business Media, 2008.

[70] A. P. Dempster, N. M. Laird, and D. B. Rubin, “Maximum likelihood from incomplete data via the em algorithm”, *Journal of the Royal Statistical Society: Series B (Methodological)*, vol. 39, no. 1, pp. 1–22, 1977.

[71] S. Yildirim, S. S. Singh, and A. Doucet, “An online expectation–maximization algorithm for changepoint models”, *Journal of Computational and Graphical Statistics*, vol. 22, no. 4, pp. 906–926, 2013.

[72] A. J. Wood, B. F. Wollenberg, and G. B. Sheblé, “Power generation, operation, and control”, John Wiley & Sons, 2013.

[73] M. Liu and G. Gross, “Role of distribution factors in congestion revenue rights applications”, *IEEE Transactions on Power Systems*, vol. 19, no. 2, pp. 802–810, 2004.

[74] D. Bertsimas, J. Pauphilet, and B. Van Parys, “Sparse regression: Scalable algorithms and empirical performance”, *Statistical Science*, vol. 35, no. 4, pp. 555–578, 2020.

[75] T. Hastie, R. Tibshirani, and R. Tibshirani, “Best subset, forward stepwise or lasso? analysis and recommendations based on extensive comparisons”, *Statistical Science*, vol. 35, no. 4, pp. 579–592, 2020.

[76] R. Tibshirani, “Regression shrinkage and selection via the lasso”, *Journal of the Royal Statistical Society: Series B (Methodological)*, vol. 58, no. 1, pp. 267–288, 1996.

[77] H. Zou, T. Hastie, and R. Tibshirani, “On the “degrees of freedom” of the lasso”, *The Annals of Statistics*, vol. 35, no. 5, pp. 2173–2192, 2007.

[78] B. Efron, T. Hastie, I. Johnstone, and R. Tibshirani, “Least angle regression”, *The Annals of statistics*, vol. 32, no. 2, pp. 407–499, 2004.

[79] H. Zou and T. Hastie, “Regularization and variable selection via the elastic net”, *Journal of the royal statistical society: series B (statistical methodology)*, vol. 67, no. 2, pp. 301–320, 2005.